



Seasonality variations in the Central Mediterranean during climate change events in the Late Holocene

M.-L. S. Goudeau^{a,*}, G.-J. Reichart^{a,b}, J.C. Wit^c, L.J. de Nooijer^b, A.-L. Grauel^{d,e}, S.M. Bernasconi^d, G.J. de Lange^a

^a Dept. of Geosciences, Utrecht University, Utrecht, The Netherlands

^b Royal Netherlands Institute for Sea Research (NIOZ), P.O. Box 59, Den Burg, Texel, The Netherlands

^c Woods Hole Oceanographic Institution, Geology and Geophysics, 266 Woods Hole Rd., Woods Hole, MA 02543, USA

^d Geological Institute, ETH Zurich, 8092 Zurich, Switzerland

^e Department of Earth Sciences, University of Cambridge, Cambridge, UK

ARTICLE INFO

Article history:

Received 19 February 2014

Received in revised form 25 October 2014

Accepted 11 November 2014

Available online 20 November 2014

Keywords:

Seasonality

Late Holocene

Central Mediterranean

Foraminiferal test chemistry

ABSTRACT

Holocene rapid climate change (RCC) events, such as the Little Ice Age (LIA), are thought to have influenced average annual temperatures only marginally, but to have affected winter temperatures relatively strongly. With summer temperatures relatively unaffected, reconstructing climate change at a seasonal resolution is crucial to fully capture Holocene climate variability. Mediterranean climate is highly seasonal, being influenced by the subtropical high-pressure belt in summer and the mid-latitude westerlies combined with outbreaks of polar winds in winter. We identified events of high- and low-detrital input to the Gulf of Taranto (Central Mediterranean Sea), anticipated to be linked to humid and dry conditions, respectively and, thereby, potentially reflecting seasonal contrasts. These events represent the Bronze Age (BA), Roman Humid Period (RHP), Medieval Climate Anomaly (MCA), LIA and present-day, and were selected for the analysis of single specimen *Globigerinoides ruber* (white) carbonate chemistry (Mg/Ca, $\delta^{18}\text{O}$ and $\delta^{13}\text{C}$). The dynamic range found for these parameters for the measured single individuals in the most recent interval reflects the present-day seasonal contrasts in temperature and precipitation, albeit with a bias towards the summer season. These results are compared with high-resolution (<15 years/sample) Sea Surface Temperature (SST) and Bottom Water Temperature (BWT) reconstructions based on the $\delta^{18}\text{O}$ of *G. ruber* (white) and Mg/Ca of benthic foraminifer *Hyalinae balthica*. Although the seasonal temperature contrast remains relatively stable, significant winter cooling is observed during the BA and LIA. Connections between high-latitude climate (winter conditions) and low-latitude climate (summer conditions) appear not straightforward during RCC events. This results in changes in the moisture balance, and in shifts in seasonal dominance between RCCs. During the LIA, winter-like conditions (cold and humid) prevail throughout the year. In contrast, winters are dry and cold during the BA, and are accompanied by dry and warm summers, suggesting year-round aridity and a relatively high seasonal temperature contrast. This could have had a profound impact on early agriculture in Southern Italy.

© 2014 Elsevier B.V. All rights reserved.

1. Introduction

Although Holocene climate has been considered as relatively stable, for specific time intervals and regions, distinct centennial to millennial scale climate variability has been recognized (Mayewski et al., 2004; Wanner et al., 2008). This variability is thought to have been instrumental in the rise and fall of past civilizations (e.g., Haug et al., 2003; Büntgen et al., 2011). The millennial scale climate events during the Holocene expressed as cold spells in the northern hemisphere are also

known as Rapid Climate Change (RCC) events (Mayewski et al., 2004). These RCC events may have affected specific parts of the climate system through deviating atmospheric patterns during certain seasons rather than impacting the year round global climate. For example, cold spells in the northern hemisphere, during RCC events as the Little Ice Age (LIA, ~150–550 cal. years BP, Grauel et al., 2013a) and the Bronze Age (BA, ~2450–3450 cal. years BP, Rohling et al., 2002, 2009; Mayewski et al., 2004), have been suggested to be primarily a winter phenomenon, implying an enhanced seasonal contrast during these periods (e.g., Denton et al., 2005). Changes in seasonality, therefore, may have played a crucial role in shaping Holocene climate variability.

High-frequency climate change has been different between regions, resulting in a complex spatial pattern, presumably reflecting interactions between low- and high-latitude climate changes (Mayewski et al., 2004;

* Corresponding author at: Department of Earth Sciences, Geochemistry, Faculty of Geosciences, Utrecht University, P.O. Box 80.021, 3508 TA Utrecht, The Netherlands. Tel.: +31 30 253.4991.

E-mail address: m.s.goudeau@uu.nl (M.-L.S. Goudeau).

Wanner et al., 2008, 2011; Mann et al., 2009). The Mediterranean lies on the boundary between the subtropical high-pressure belt and the mid-latitude westerly system (Fig. 1a). During summer the Mediterranean region is under the influence of subtropical climate, which is closely linked to the position of the Inter-Tropical Convergence Zone (ITCZ; e.g., Alpert et al., 2006). In contrast, during winter the subtropical conditions are displaced southward and the Mediterranean region is primarily connected to the mid-latitude climate phenomena such as the westerly system (Trigo et al., 2006). Together, this results in relatively mild, humid winters and warm, dry summers. The Mediterranean therefore provides an ideal setting for investigating interactions between high- and low-latitude climate variability (Alpert et al., 2006; Trigo et al., 2006), but at the same time requires reconstructions at a seasonal scale. Precipitation records from the Mediterranean area indicate both increased droughts and floods during the LIA, suggesting an enhanced contrast between dry summer conditions and winter precipitation (e.g., Grove, 2001; Mann et al., 2009). Relatively humid conditions during the reign of the Romans, the Roman Humid Period (RHP, 1950–2400 cal. years BP, Grauel et al., 2013b), are generally associated with a more southern pathway of the westerlies, increasing

winter precipitation in the region (Dermody et al., 2012). In general, observed millennial scale climate variability in the Northern Mediterranean during the Holocene has been explained by changes in extent of high northern latitude climate during winter (Rohling and Pälike, 2005; Peyron et al., 2011; Comboutrieu-Nebout et al., 2013).

Understanding seasonality (the seasonal contrast between summer and winter) is, however, not only vital for understanding the physical processes underlying short-term climate change, but is also important for unraveling proxy records, which may show a seasonal bias. Most proxies for sea surface temperature (SST) or sea surface salinity (SSS) are influenced by several environmental parameters, of which seasonality is one. Distinguishing between shifts in seasonality and the other parameters is, therefore, often difficult (Grauel et al., 2013a).

Here we use a sediment core from the Gulf of Taranto (Fig. 1b, Central Mediterranean) to reconstruct past changes in seasonality from selected time slices, using both novel and more traditional approaches. Recently Wit et al. (2010) showed that Mg/Ca values measured on single specimens of the planktonic foraminifer *Globigerinoides ruber* (white) reflect the year round fluctuations of SST in the Mediterranean Sea. As precipitation patterns in the Mediterranean are highly seasonal

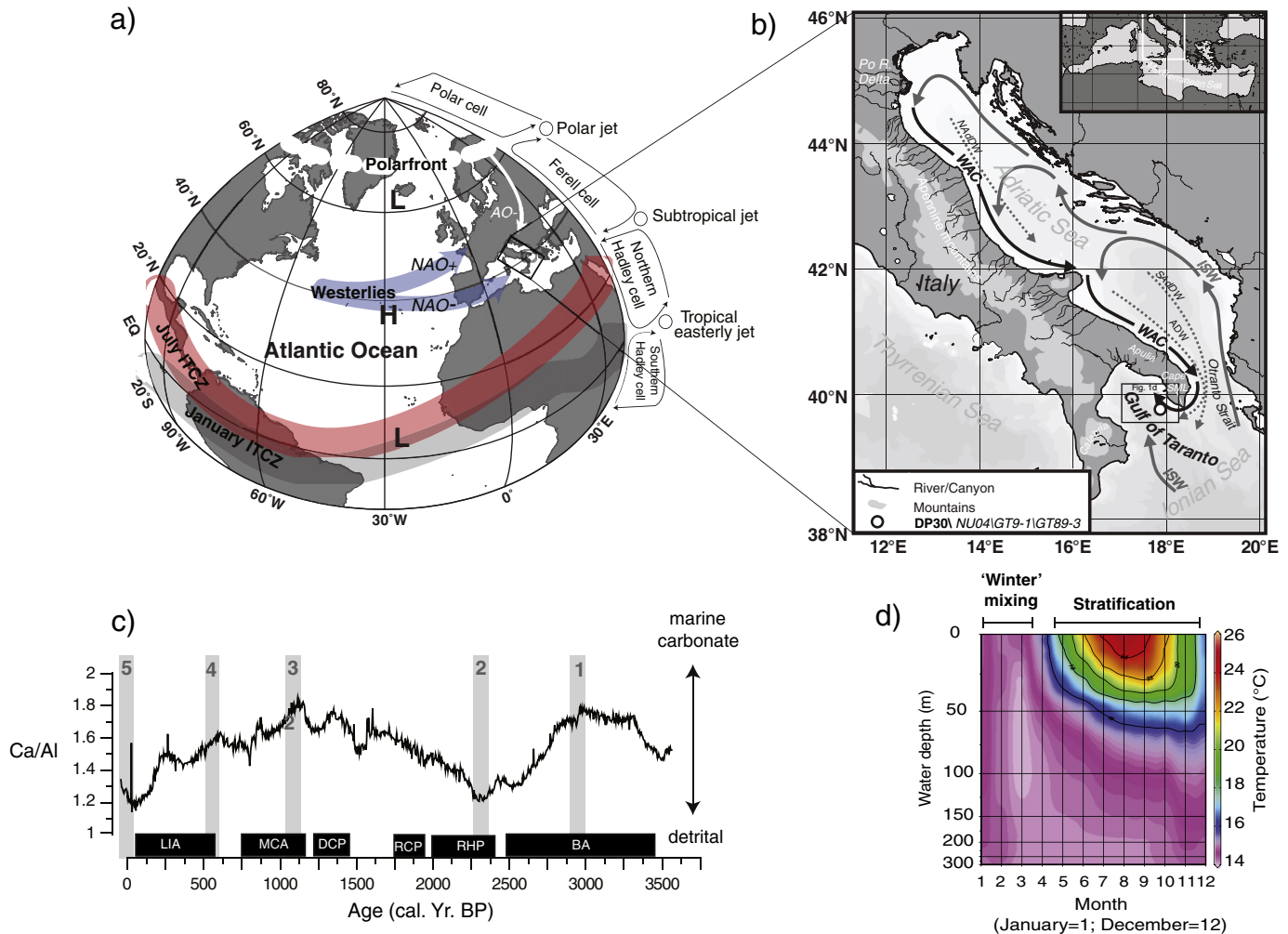


Fig. 1. (a) Atmospheric circulation patterns in the northern hemisphere influencing climate in the study area. AO—is negative Arctic Oscillation, NAO is Northern Atlantic Oscillation, NAO+ reflects the precipitation pattern under a positive mode and NAO— the precipitation patterns when the NAO is in a negative mode. ITCZ stands for the Inter Tropical Convergence Zone. H is high pressure cell, and L is low pressure cell. (b) Map of the study area showing the Adriatic Sea and Ionian Sea, general water circulation and water masses (WAC—Western Adriatic Current; nADW, sADW, and ADW are North-, South-, and Adriatic deep water, ISW is Ionian Surface Water), and the core locations in the Gulf of Taranto discussed in this study (adapted after Grauel et al., 2013a). (c) The Ca/Al ratio of the sediments of core DP30 (Goudeau et al., 2014) with the intervals (gray bars) selected for individual *G. ruber* (white) test chemistry (see Table 1). Dark rectangles correspond to various periods mentioned in the text: Bronze Age (BA, Mayewski et al., 2004) and the Roman Humid Period (RHP), Roman Classical Period (RCP), Medieval Climate Anomaly (MCA) and Little Ice age (LIA) as defined by Grauel et al. (2013b). (d) The monthly distribution of water column temperatures in the Gulf of Taranto (Locamini et al., 2010; data retrieved from world ocean atlas, 2009, <http://www.nodc.noaa.gov>), averaged for 38.875°N/17.125°E–40.375°N/18.375°E (adapted after Grauel et al., 2013a).

we apply this technique to a number of time slices, which show low- or high-detrital input and, therefore, maximal seasonal contrast. These time slices correspond to climate periods as the BA, RHP, Medieval Climate Anomaly (MCA, ~750–1150 cal. years BP, Stine et al., 2000; Grauel et al., 2013b) and LIA. The relatively high sedimentation rates in this area create an ideal setting for high-resolution studies (e.g., Cini Castagnoli et al., 1990). Results from the Mg/Ca, $\delta^{18}\text{O}$ and $\delta^{13}\text{C}$ analyses on single specimens of *G. ruber* (white) were compared to several more established proxy records: pooled $\delta^{18}\text{O}$ and $\delta^{13}\text{C}$ from *G. ruber* (white) (extended from Grauel et al., 2013b), U^{k}_{37} (Versteegh et al., 2007; Grauel et al., 2013a) and Mg/Ca of the benthic foraminifera *Hyalinea balthica* (this study). Previous studies from the Gulf of Taranto showed that the bulk test chemistry of *G. ruber* (white) reflects summer conditions, whereas U^{k}_{37} records reflect winter/spring temperatures. *H. balthica* (Schroeter, 1783) is a primarily neritic to upper bathyal benthic foraminiferal species (<600 m) exhibiting an unusual high temperature sensitivity that is ~4 times higher than observed for other benthic foraminiferal species (Rosenthal et al., 2011), making this species ideal for bottom water temperature reconstructions (Wit et al., 2012). As bottom water temperatures in the Gulf of Taranto are set in winter (see Section 2.2), we suggest that the Mg/Ca of specimens of *H. balthica* reflects winter temperature. In addition, combining temperature proxies with stable oxygen isotopes allows deconvolving the oxygen isotopic composition of the sea water and hence precipitation, which is highly seasonal in the Mediterranean. Results provide a high-resolution multi-proxy record of seasonality for both precipitation and temperature for the last 3500 years in the Gulf of Taranto.

2. Study area

2.1. Present climate

Changes in winter temperature and precipitation in the north-eastern Mediterranean have been related to high-latitude climate change (e.g., Rohling et al., 2002; Giraudi et al., 2011). A stronger Siberian High enhances cold Bora winds from the north, affecting the Adriatic SST (Fig. 1a; Rohling et al., 2002). Winter precipitation in Italy is modulated by the North Atlantic Oscillation (NAO), which changes the route of the westerlies over Europe. During a positive phase of the NAO, the westerlies follow a more northward track and less winter precipitation reaches Italy (Fig. 1a; Hurrell, 1995; Brandimarte et al., 2011). In contrast, Mediterranean summers are influenced by low latitude climate patterns (Pierivitali et al., 1997; Alpert et al., 2006). An important feature of low latitude climate is the so-called Inter Tropical Convergence Zone (ITCZ), where the northern and southern Hadley cells collide (Fig. 1a). During summer, the position of the ITCZ moves north and the high-pressure field of the associated northern Hadley cell shifts over the Mediterranean, resulting in dry and warm conditions (Alpert et al., 2006). Hence, the Mediterranean is characterized by high seasonality, both in temperature and precipitation.

2.2. Modern day oceanography and sedimentary dispersion patterns

The Gulf of Taranto is located between the two southern Italian regions Apulia and Calabria, in the north-western Ionian Sea (Fig. 1b). Large amounts of sediments are transported to the Gulf of Taranto from the Adriatic Sea by the West Adriatic Current (WAC; Fig. 1b; Turchetto et al., 2007; Goudeau et al., 2013). This WAC has a relatively low salinity as it is fed by freshwater runoff from the Po river and several smaller Alpine and Apennine rivers (Turchetto et al., 2007). In the Gulf of Taranto, the surface water from the low-salinity and nutrient-rich WAC mixes with the more saline, nutrient-poor Ionian Surface Waters (ISW) from the south (Fig. 1b, Poulain, 2001; Morovic et al., 2006).

During summer an anti-cyclonic atmospheric circulation prevails over the Mediterranean, which is related to the northward displacement of the North African Hadley cell and which in turn is part of the

ITCZ (Pierivitali et al., 1997; Alpert et al., 2006). Hence, the summer season is characterized by warm and dry conditions. Subsequently, river discharge is reduced during this season (Alpert et al., 2006) and thus also the influence of the WAC in the Gulf of Taranto (Poulain, 2001). The highest discharge and cooling, and hence the largest extent of the WAC are associated with the winter season (Sellschopp and Álvarez, 2003). During winter, westerly winds penetrate more southward, enhancing transport of moist air from the Atlantic Ocean to the Mediterranean (Brandimarte et al., 2011). This corresponds to a more positive mode of the North Atlantic Oscillation (NAO) during winter (e.g. Fig. 1a; Hurrell, 1995). In addition, during winter a positive Siberian high potentially stimulates outbreaks of cold polar air from the north, also known as the Bora (Fig. 1a). Cooling increases the formation of deep water in the Northern Adriatic, the northern Adriatic Deep water (nADW, Fig. 1b) and the Southern Adriatic, Southern Adriatic Deep water (sADW, Fig. 1b). More intense deep water formation increases ventilation of bottom waters in the Adriatic and the Gulf of Taranto. In addition, the SST decrease during winter results in the convective overturning of the water column in the Gulf of Taranto that subsequently remains stratified throughout the summer (Zonneveld et al., 2008).

3. Material and methods

3.1. Core site and age model

Multicore NU-04 (39.764°N/17.892°E, water depth 160 m) was recovered during the RV Universitatis cruise 'ESPRESSO' in 2005 (Fig. 1b). Sampling of the core material for sediment and foraminifera was performed at a resolution of 3 mm. The nearby piston core DP30 (39.835°N/17.801°E), with a total length of 8.5 m was recovered from a water depth of 270 m below sea level (m.b.s.l.) during the RV Pelagia cruise 'DOPPIO' in 2008 (Fig. 1b). This core was sampled at a 2.5 mm resolution except for the top 20 cm, which was sampled at a 5 mm resolution. Samples were split for geochemical analyses and foraminiferal studies. For dating purposes ^{210}Pb was determined for the top part of the nearby core NU-04 and DP30 at the laboratories of CEAC, Cuba and the Royal Netherlands Institute for Sea Research (NIOZ, Texel, Fig. 2).

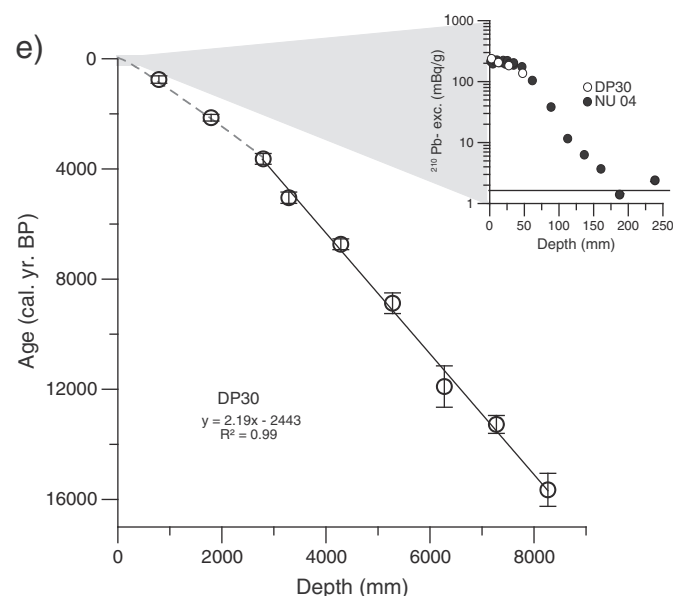


Fig. 2. Age model of DP30. The calibrated ^{14}C -ages and their standard deviation (shown in the lower panel) were calibrated with the program OxCal v3.10 (Ramsey et al., 2009), with the references of atmospheric data from Reimer et al. (2004) and the curve Marine04 with the marine data from Hughen et al. (2004; $\Delta R = 121 \pm 60$ years). In the upper panel the ^{210}Pb depth profile of NU-04 (black circles) and DP-30 (white circles) was used to date the upper part of the core.

In addition 3 bulk planktonic foraminifera samples of core DP30 and one from the bottom of NU-04 were picked and analyzed for ^{14}C (MICADAS, Ruff et al., 2007; Synal et al., 2007, Fig. 2) at the AMS Radiocarbon Dating Laboratory at ETH Zurich. ^{14}C -ages were calibrated using the program OxCal v3.10 (Bronk Ramsey et al., 2009) with the Marine04 calibration curve (Hughen et al., 2004) with an additional regional reservoir correction of 121 ± 60 (ΔR).

Using a model (Boer et al., 2006) with a background of 15 Bq/kg, a sedimentation rate of 0.85 mm/year with a bioturbation layer of 4.4 cm was determined for the upper part of core NU-04. This model for the upper-most part of the sediment was combined with a ^{14}C date and compared to the cumulative sediment accumulation taking the effects of increasing water content in the upper part into account. A 1st order polynomial was used to combine ^{210}Pb and ^{14}C ages. During the recovery of DP30, the upper few mm were lost. Comparison between the ^{210}Pb profile of DP30 and NU-04 revealed that this was equivalent to a loss of ~10 years (Fig. 2). For the age model of DP30 we assumed a linear relationship between cumulative sediment accumulation and ^{14}C dates (Fig. 2). The age models for NU-04 and DP30 are described in more detail in Grauel et al. (2013a) and Goudeau et al. (2014).

3.2. Bulk geochemistry

To establish the Ca/Al record, sediment samples were freeze-dried and powdered using an agate mortar. From every powdered sample, 125 mg of material was dissolved in 2.5 ml HF (40%) and 2.5 ml pre-mixed acid (HNO_3 16.25% and HClO_4 45.5%) and heated at 90 °C in a closed vessel for at least 8 h. Subsequently, the lid was removed and the samples were evaporated at 160 °C until a gel was formed. The gels were then dissolved in 25 ml 1 M HNO_3 . These dissolved samples were analyzed for their major and minor elemental composition using inductively coupled plasma-atomic emission spectroscopy (ICP-AES) with a Perkin Optima 3000 at Utrecht University. Relative precision (<5%) and accuracy were established by duplicates, in-house and international standards (ISE-921). For a full description and interpretation of the Ca/Al record see Goudeau et al. (2014).

3.3. Foraminifera

Samples were sieved into size fractions of 125–200 μm , 200–250 μm , 250–355 μm and >355 μm for foraminifera studies. From these fractions foraminifera tests were selected for stable isotope and trace metal analyses as listed below.

3.3.1. Single foraminiferal test chemistry of *G. ruber* (white) ($\delta^{18}\text{O}$, $\delta^{13}\text{C}$ and Mg/Ca)

For the foraminiferal single specimen test chemistry of *G. ruber* (white) ($\delta^{18}\text{O}$, $\delta^{13}\text{C}$ and Mg/Ca), we selected intervals covering both

maximum and minimum values from the downcore Ca/Al record of core DP30 (see Fig. 1c, Table 1, Goudeau et al., 2014). The Ca/Al ratio reflects variability between marine biogenic carbonate (Ca) and terrestrial (Al) inputs and is, therefore, thought to reflect changes in run-off and precipitation (e.g. Goudeau et al., 2013; Goudeau et al., 2014). As precipitation in the Mediterranean region is highly seasonal, we expect that differences in seasonal contrast are maximal between samples with contrasting high and low run-off and precipitation. Intervals for reconstructing seasonality were selected as to maximize the range in seasonality. Intervals with high Ca/Al values (i.e. low terrestrial input, intervals 1 and 5) are expected to show a limited seasonal contrast. Intervals characterized by low Ca/Al values (i.e. high terrestrial input, intervals 2 and 4) or intermediate values (interval 3) are expected to show a stronger seasonal contrast.

The intervals used for single specimen analyses were restricted to approximately 50 years, corresponding to intervals of ± 3 cm (i.e. 12 samples), to limit the effect of inter-annual variability, as well as centennial scale climate variability (Table 1). These intervals (Fig. 1c, Table 1) correspond to different recognized climate periods: the Bronze Age (1, BA), the Roman Humid Period (2, RHP), the Medieval Climate Anomaly (3, MCA) and the Little Ice Age (4, LIA).

From these intervals up to 30 single *G. ruber* (white) tests were picked for single specimen Mg/Ca analysis using laser ablation-ICP-MS. Because of the limited number of available specimens in the 200–355 μm size fraction, also larger individuals (355–400 μm) are included in the single specimen analysis for the RHP and MCA interval. Samples were pre-cleaned in a similar way as for the isotope analysis but without crushing the foraminiferal tests. Limited test size of individual specimens did not allow for multiple measurements on one single chamber. Therefore, the 3 last-formed chambers per specimen were ablated with a deep-ultraviolet wavelength laser (193 nm) using a Lambda Physik excimer laser system with GeoLas 200Q optics. The carbonate test was ablated with an 80 μm spot diameter and a pulse repetition rate of 5 Hz for approximately 30–60 s with an energy density of approximately 1 J/cm². Ablated material was transported on a He gas flow and mixed with argon before being introduced into the ICP-MS plasma. Element to calcium ratios were quantified using ^{24}Mg , ^{26}Mg , ^{27}Al , ^{42}Ca , ^{43}Ca , ^{44}Ca , ^{55}Mn , and ^{88}Sr isotopes and their relative natural abundances on a sector field ICP-MS (Thermo Finnigan Element 2). Elemental ratios were based on averaging counts for each ablation profile. Calibration is performed against the U.S. National Institute of Standards and Technology SRM N610 glass (ablated at an energy density of approximately 5 J/cm²) using values from Jochum et al. (2011) and checked with an in-house matrix matched calcite standard GJR (ablated at ~1 J/cm²) using ^{43}Ca as an internal standard (Reichert et al., 2003). Using different ablation energies between glass standard and calcite samples was shown to not affect accuracy (Dueñas-Bohórquez et al., 2011). Measurements were checked for possible remaining traces of surface contamination

Table 1

Overview of samples: name, age interval, depth interval (cmbs = cm below seafloor), number of individuals (N) used for individual single spec *G. ruber* test chemistry and the average $\delta^{18}\text{O}$ of *G. ruber* in the interval based on the pooled specimens and the individual specimens.

# (Fig. 1c)	Period total age interval (cal. years BP) ^a	Sampled interval (cal. years BP)	Sampled interval depth (cmbs) (bottom-top)	N	$\delta^{18}\text{O}$ (downcore) average	$\delta^{18}\text{O}$ (individuals) average
1	Bronze Age (BA) (3450–2450 cal. years BP)	2982–2932	234–237	29	0.67	0.60
2	Roman Humid Period (RHP) (2400–1950 cal. years BP)	2316–2269	190–186	30	0.66	0.26 ^b
3	Medieval Climate Anomaly (MCA) (1150–750 cal. years BP)	1067–1115	990–953	31	0.67	0.62
4	Little Ice Age (LIA) (550–100 cal. years BP)	572–522	574–536	30	0.98	0.78
5	Present	46 to –5 cal. years BP (1904–1958 AD)	111–44	32	0.83	0.60

^a Total age interval for intervals of climate events as reported in Mayewski et al. (2004) (BA) and Grauel et al. (2013b) (RHP, MCA and LIA).

^b The single spec *G. ruber* test chemistry and the average $\delta^{18}\text{O}$ of *G. ruber* in the interval based on the pooled specimens differ (see text).

by evaluating Al and Mn profiles acquired during ablation. Any remaining clay particles or post-depositional Mn-rich inorganic coatings that are usually also enriched in Mg potentially influence the detected Mg/Ca value, thus biasing foraminiferal Mg/Ca values. Therefore, data with elevated Al/Ca (>2.0 cps/cps) and Mn/Ca (>0.6 cps/cps) counts were excluded. After Mg/Ca analysis with LA-ICP-MS, the same specimens were analyzed individually for stable carbon and oxygen isotopes, using the method described later in Section 3.3.2 for the bulk *G. ruber* (white) samples. Because of smaller sample size, the reproducibility of these measurements was $\pm 0.15\%$.

As not all data sets were of a similar size (n) a Kruskal–Wallis test (a non-parametric ANOVA) was performed, using the software PAST to identify whether differences between sample population medians were significant (Hammer et al., 2001). To test whether the individual samples in each time slice come from populations with different variances, i.e. the homogeneity of variances, a Bartlett's test was performed (Snedecor and Cochran, 1989). With a Bartlett's test the null hypothesis 'all tested population variances are equal' is tested. Both the Kruskal–Wallis and Bartlett's tests demand normal distributed data sets. To test for normality we performed a Shapiro–Wilk test (Shapiro and Wilk, 1965).

Mg/Ca values for *G. ruber* (white) were converted to temperature (T) using the calibration of Elderfield and Ganssen (2000):

$$\text{Mg/Ca} = 0.52 \exp(0.10T). \quad (1)$$

Using the calibration of Anand et al. (2003) values would result in somewhat higher temperatures, especially at the higher end of the observed range in Mg/Ca. Although these values are not unrealistic (see also discussion in Wit et al., 2010), the Elderfield and Ganssen (2000) calibration results in average temperature more closely to the oxygen isotope based averages.

Using the average Mg/Ca temperature (Eq. 1) and $\delta^{18}\text{O}_c$ measured on the same specimens, $\delta^{18}\text{O}_w$ was calculated by taking advantage of the truly paired data set (resulting from analyses of the same specimen). We do realize that combining stable oxygen isotope analyses with Mg/Ca based temperatures may cause a major propagation of errors (Schmidt, 1999; Rohling, 2000). Therefore, we consider the values obtained as semi-quantitative only.

The $\delta^{18}\text{O}_w$ was correlated to sea surface salinity (SSS) for the region using the Eq. (3) of Wit et al. (2010), which is based on the data from Pierre (1999) and Schmidt et al. (1999):

$$\delta^{18}\text{O}_w = 0.285 * \text{SSS} - 9.47. \quad (2)$$

Converting $\delta^{18}\text{O}_w$ values from VSMOW values to VPDB values was corrected for by addition of 0.27‰ (Hut, 1987).

3.3.2. $\delta^{18}\text{O}$ and $\delta^{13}\text{C}$ downcore analysis of *G. ruber* (white)

For $\delta^{18}\text{O}$ and $\delta^{13}\text{C}$ downcore analysis of *G. ruber* (white), twenty specimens were picked under the microscope from the 200–355 μm fraction of every 4th sample (i.e. 1 cm resolution instead of a 2.5 mm resolution) between 2050 and 2800 mm depths. Results from the upper part of the core (0–2050 mm depth) were previously reported in Grauel et al. (2013b). To avoid variations in $\delta^{18}\text{O}$ and $\delta^{13}\text{C}$ caused by different morphotypes of *G. ruber* (white), we selected only the morphotype *platys* according to the nomenclature of Numberger et al. (2009). After picking, foraminiferal tests were cleaned according to the protocol described by Grauel and Bernasconi (2010), in order to eliminate carbonate particles adhering to the shell surface. For isotope analyses, about 150–200 μg of cleaned shell material was dissolved under vacuum with two drops of $\sim 103\%$ H_3PO_4 at 70 °C cleaned cryogenically using a Thermo Fisher Kiel IV preparation device coupled to a Thermo Fisher MAT 253 mass spectrometer. The reproducibility of the $\delta^{13}\text{C}$ and $\delta^{18}\text{O}$ analysis is based on repeated measurements of the MS2 in-house standard, and calibrated to the

international standards NBS19 ($\delta^{13}\text{C}_{\text{VPDB}} + 1.95\%$, $\delta^{18}\text{O}_{\text{VPDB}} - 2.2\%$) and L-SVEC ($\delta^{13}\text{C}_{\text{VPDB}} - 46.6\%$, $\delta^{18}\text{O}_{\text{VPDB}} - 26.41\%$), which was better than 0.1‰ (1 σ). All $\delta^{13}\text{C}$ and $\delta^{18}\text{O}$ results are reported in the conventional delta notation relative to VPDB.

To check for consistency between the new data presented here (samples between 2050 and 2800 mm) and previously reported stable isotope analyses of *G. ruber* (white) for the same core (samples between 0 and 2050 mm; Grauel et al., 2013b) we compared averages and standard deviations. To do so we need to take into account the lower resolution of the new data set (the standard error of the mean (SE)), thus we correct the standard deviation (σ) by Eq. (3).

$$\text{SE} = (\sigma/\sqrt{n}) \quad (3)$$

with n representing the difference in resolution ($n = 4$).

To transfer the oxygen isotope value to SST we used the paleotemperature equation of O'Neil et al. (1969) as refitted by Shackleton (1974):

$$T = 16.9 - 4.38 * (\delta^{18}\text{O}_c - \delta^{18}\text{O}_w) + 0.1 * (\delta^{18}\text{O}_c - \delta^{18}\text{O}_w)^2, \quad (4)$$

with T representing temperature in °C, $\delta^{18}\text{O}_c$ the $\delta^{18}\text{O}$ of the carbonate shells, and $\delta^{18}\text{O}_w$ the $\delta^{18}\text{O}$ of ambient seawater. Initially we take a constant $\delta^{18}\text{O}_w$ of 1.4‰, the modern water value in the Gulf of Taranto (Grauel and Bernasconi, 2010), however, later in the discussion we also evaluate changes of $\delta^{18}\text{O}_w$ over time.

3.3.3. *H. balthica* Mg/Ca

For Mg/Ca analysis of *H. balthica*, between 7 and 10 specimens from the 125–250 μm size fraction were selected from every 4th sample, i.e. one sample each cm instead of every 2.5 mm, of core DP30 and every 1.2 cm instead of every 3 mm of core NU04. When a sample contained less than 7 foraminifera it was combined with the sample directly following it downcore. This was primarily needed for the upper 1.5 m of core DP30. Samples were cleaned following the protocol by Boyle and Keigwin (1985) and modified after Rosenthal et al. (1997) and Goudeau (2014). This involved four cleaning steps to remove clays, organic matter and metal oxides: first samples are cleaned ultrasonically, followed by a treatment in a hot basic reducing solution (0.25 M citric acid in 16 M ammonia made up to 1 M in hydrazine) and a hot basic oxidizing solution (1% H_2O_2). The cleaning process is completed with multiple dilute acid leaches (0.001 M HNO_3).

To obtain an optimal dilution factor, samples with low amount of specimens (<8 individual foraminifera) were dissolved in 2 ml 0.1 M HNO_3 , while samples with >8 individual foraminifera were dissolved in 3 ml 0.1 M HNO_3 . Elemental composition of the samples (Mg, Ca, Na, Al and Mn) was analyzed with a high resolution ICP-MS (Element 2, Thermo Fischer Scientific) equipped with a double spray chamber and Teflon micro-flow nebulizer. Relative precision (<4%) was determined by multiple measurements on international (ECRM-752-1) and in-house standards (GJR and CMSI). Every measurement consumed 1.8 ml of solution. The remainder was used for duplicate analyses: the samples were diluted to 10 ppm of calcium by adding 0.1 M HNO_3 . To correct for a variable calcium matrix a 3-D ratio calibration method was used (Rosenthal et al., 1999). For this, five standards with fixed calcium concentration were measured for a suite of dilutions (5, 10, 20, 30, 50 and 100 ppm calcium matrix).

Mg/Ca values were converted to temperature values using the exponential equation of Rosenthal et al. (2011):

$$\text{Mg/Ca} = 1.327 \exp(0.123) \text{ BWT}. \quad (5)$$

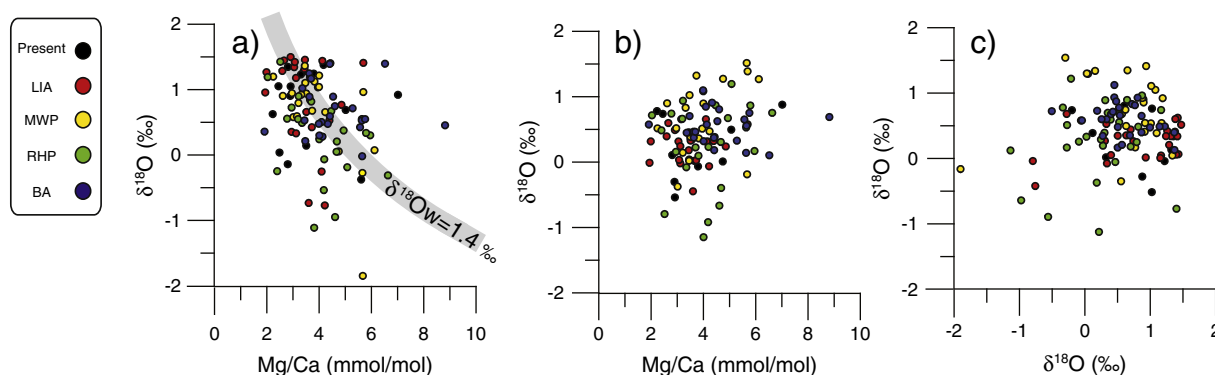


Fig. 3. The individual measured *G. ruber* (white) tests Mg/Ca versus $\delta^{18}\text{O}$ (a) and $\delta^{13}\text{C}$ (b) and $\delta^{13}\text{C}$ versus $\delta^{18}\text{O}$ (c). The gray line in (a) represents the correspondence between temperature and $\delta^{18}\text{O}$ and Mg/Ca when the $\delta^{18}\text{O}_w$ equals 1.4‰.

4. Results

4.1. Single specimen *G. ruber* (white) test chemistry

G. ruber (white) stable isotopes of single specimens vary between -2‰ and 3.0‰ for carbon and from -4 to 1.6‰ for oxygen isotopes (Figs. 3 and 4). The latter correspond to SSTs varying between 16°C and 32°C (Figs. 4c and 6a) using Eq. (1). Mg/Ca values of the entire data set vary between 1.28 and 9 mmol/mol, based on averaging 3 single chamber measurements per single specimen (Figs. 3 and 4). Calculated sea surface temperatures indicate a range from ~ 13 to 28.3°C (Fig. 4b).

The Shapiro–Wilk test identifies all individually measured $\delta^{18}\text{O}$, $\delta^{13}\text{C}$ and Mg/Ca as normally distributed, except the $\delta^{18}\text{O}$ of the samples from the MCA, the LIA and the most recent interval. Therefore, a Kruskal–Wallis and a Bartlett's test were performed only for the RHP and the BA intervals of the $\delta^{18}\text{O}$ datasets. The Kruskal–Wallis test of *G. ruber* (white) Mg/Ca indicates that the median for the BA samples is significantly higher than for all other samples (Table 2). Furthermore, the LIA has significantly lower Mg/Ca based SST than the RHP. The Bartlett's test has a p-value larger than 0.05 indicating that the ranges of all the sampled intervals of Mg/Ca based SSTs are not significantly different. The Kruskal–Wallis test of the oxygen isotopes for the BA and the RHP interval indicates that their medians are significantly different (Table 2). Testing with Bartlett's test reveals that there are no significant changes in the range of oxygen isotope values between the BA and RHP interval ($p > 0.05$). The *G. ruber* (white) carbon isotope median during the MCA is significantly higher than that from the RHP, LIA, and present (Table 2). Furthermore, the *G. ruber* (white) carbon isotope median during the BA is significantly higher than that during the LIA. Bartlett's test reveals a significant difference between the range of the different intervals at $p < 0.01$ (with a $\text{Chi}^2 = 23.87$).

No correlation is found between individual *G. ruber* (white) Mg/Ca, $\delta^{18}\text{O}$ and $\delta^{13}\text{C}$ (Fig. 3). Average values based on individuals, however, are in line with the downcore record based on pooled specimens (Fig. 5a). Mg/Ca-based SSTs correspond to stable oxygen isotope-based temperatures for all intervals, except during the BA (Fig. 4a). For all intervals, average carbon isotope values of the individuals correspond to the average downcore values.

4.2. Stable isotopes ($\delta^{18}\text{O}$, $\delta^{13}\text{C}$) of pooled *G. ruber* (white) specimens

The oxygen isotopes of *G. ruber* (white) from this study (about 20 species pooled for a single analysis) vary between 1.2‰ and 0.4‰ and have an average value of 0.8‰ VPDB (not shown). The pooled downcore oxygen isotope data corresponds to temperatures between ~ 18 and 22°C , using Eq. (4) (Fig. 5a). Taking the lower sample resolution of our present data relative to previously reported data for the upper part of the core into account (Grauel et al., 2013b) the new series and the

previous data set have similar standard errors ($\text{SE} = 0.15$ and 0.25 , respectively).

The carbon isotopes of *G. ruber* (white) from this study vary between -0.4‰ and 1.2‰ (average = 0.79 , Fig. 5b). The standard deviation, taking the lower resolution of our samples into account, indicates that new and previous carbon isotope data also have similar standard errors ($\text{SE} = 0.20$ and 0.26 respectively). The oxygen and carbon isotope records do not display significantly different values between the lower and higher resolution series (Fig. 5a, b).

4.3. *H. balthica* Mg/Ca

For all samples of *H. balthica*, Fe/Ca and Mn/Ca were monitored to check for contamination. For all samples, these values were below 40 and 0.6 cps/cps respectively and, therefore, the impact of contamination on determined Mg/Ca was considered negligible. The Mg/Ca values for *H. balthica* vary between 7.5 and 12 mmol/mol, corresponding to sea water temperatures ranging from ~ 14.5 to 17°C using Eq. (5) (Figs. 5a and 6). Variability between samples is thus higher than the analytical error for measuring.

In core NU-04 reconstructed temperatures of the bottom waters show a peak from 1940 until 2000 years AD (Fig. 6). Relatively higher reconstructed temperatures from the DP30 core are found around 300, 1350–1650, 1800–2500, around 2550 and 2450–3450 cal. years BP (Fig. 5a). Low BWTs ($\sim 15^\circ\text{C}$ and below) based on Mg/Ca of *H. balthica* are found between 2550 to 2700 cal. years BP (Fig. 5a).

5. Discussion

5.1. Proxies to reconstruct seasonal contrasts

5.1.1. Single specimen *G. ruber* (white) test chemistry (Mg/Ca and oxygen isotopes) as a proxy for seasonal temperature and precipitation range

The planktonic *G. ruber* (white) inhabits the upper part of the water column (Waelbroeck et al., 2005) and its test chemistry (Mg/Ca and $\delta^{18}\text{O}$) from surface sediments in the Mediterranean Sea reflects present-day seasonality (Wit et al., 2010). In the Gulf of Taranto *G. ruber* (white) is thought to thrive mainly during the warm summer season (Grauel and Bernasconi, 2010). Nevertheless, it is also known to reproduce throughout the year (Pujol and Grazzini, 1995; Bárcena et al., 2004), and hence its test chemistry should reflect the full annual cycle, albeit biased towards summer conditions.

Present-day sea surface temperatures in the Gulf of Taranto range from 14°C in winter to 24°C during summer (Fig. 1d). The Mg/Ca-based temperature estimates, derived from single specimens of *G. ruber* (white) for the most recent time slice (1905–1955 AD) show a similar range (15 – 26°C , Figs. 3, 4 and 5a). The median of the reconstructed temperatures ($\sim 20^\circ\text{C}$) reflects a bias towards summer season SSTs, in line with *G. ruber* (white) productivity (Fig. 4b). In view of

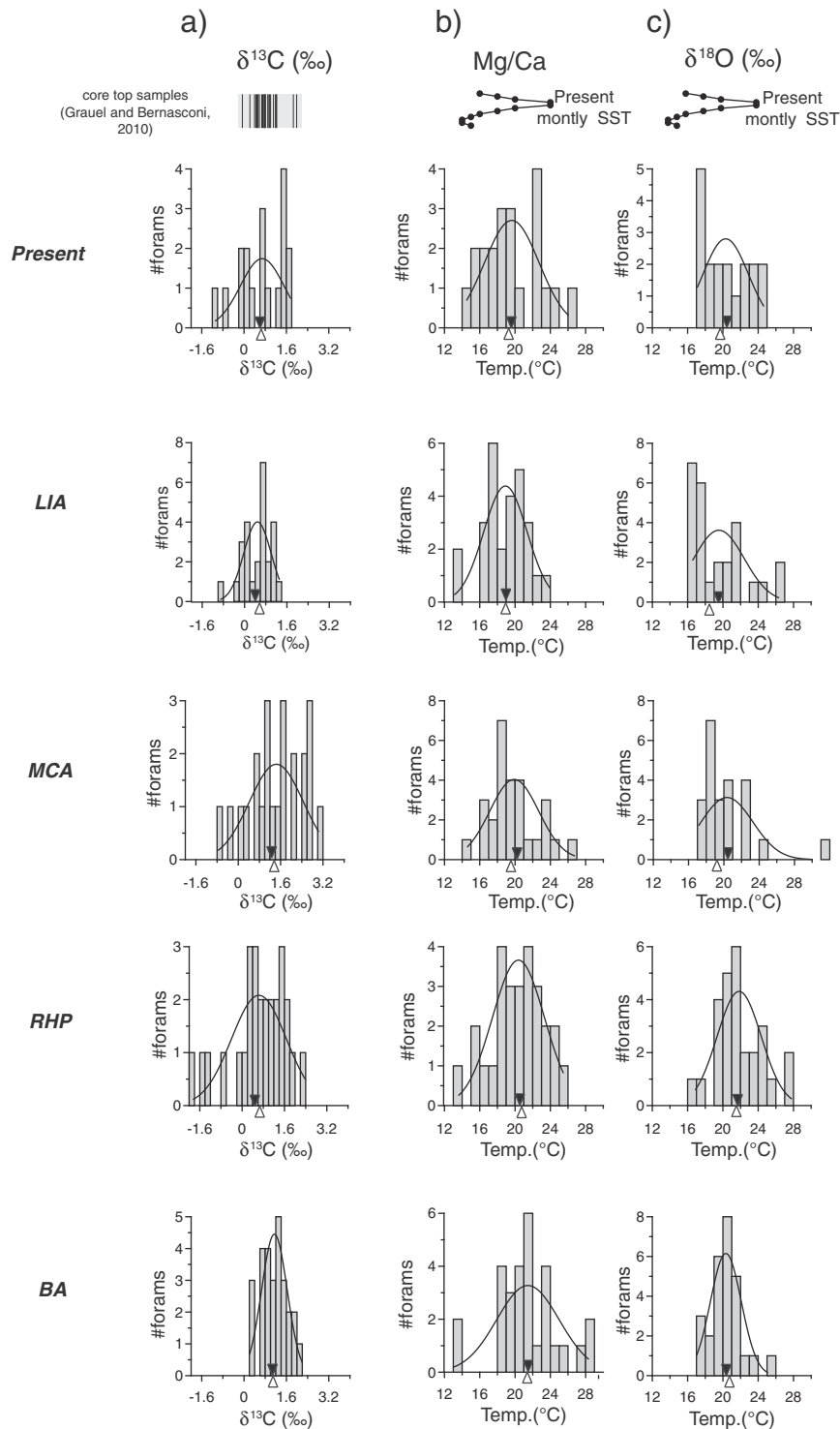


Fig. 4. Histogram of the different time slices of (a) the individual *G. ruber* (white) $\delta^{13}\text{C}$ compared to the *G. ruber* (white) $\delta^{13}\text{C}$ as found in the core top samples in the Gulf of Taranto and south-western Adriatic coast (Grauel and Bernasconi, 2010) as well as SST based on Mg/Ca (b) and $\delta^{18}\text{O}$ (c) of individual *G. ruber* (white) compared to measured present day monthly SST in the Gulf of Taranto (see Fig. 1d). Black triangles represent the average, and white triangles the median. Please note that the indicated time interval represents that for our samples and not the full climate period.

sedimentation rate and interval taken, each sample represents ~50 years; consequently, inter-annual variability will also affect the reconstructed temperature range. However, the good fit with the present-day seasonal range indicates that primarily seasonality is recorded.

The range of SSTs based on oxygen isotopes (16 to 26 °C, Fig. 4c) measured on the same *G. ruber* (white) specimens that were analyzed for Mg/Ca is also similar to that of today. Hence, both Mg/Ca and the

oxygen isotopes of individually measured *G. ruber* (white) are in line with the present-day seasonal range. Plotting the oxygen-isotope-based temperatures for individual specimens against the Mg/Ca values of the same individuals, however, shows only a weak correlation (Fig. 3a). This implies that other factors than temperature also affect either one or both proxies on the level of individuals. In addition to temperature, Mg/Ca and oxygen isotopic values of foraminifera tests

Table 2

Kruskal–Wallis test for the different proxies of the individual measured *G. ruber* (white) species. If $p < 0.05$ (in bold) then the null hypothesis $\mu_k = \mu_y$ is false (with μ being the median of the sample); these are the significant results. If the data set did not have a normal distribution and thus no Kruskal–Wallis test could be performed this is indicated with an x.

Proxy	Period	RHP	MCA	LIA	Present
Temp. Mg/Ca	BA	0.32	0.05	0.001	0.04
	RHP		0.59		0.35
	MCA			0.28	0.53
	LIA				0.66
Temp. $\delta^{18}\text{O}$	BA	0.02	x	x	x
	RHP		x	x	x
	MCA			x	x
	LIA				x
$\delta^{13}\text{C}$	BA	0.22	0.21	0	0.1
	RHP		0.04	0.1	0.75
	MCA			0	0.02
	LIA				0.26

are also influenced by salinity and sea water carbonate chemistry (e.g., Dueñas-Bohórquez et al., 2009; Dissard et al., 2010; Wit et al., 2010; Hönisch et al., 2013). In the study area, salinity potentially plays an appreciable role as it is located at the end of the relatively low-salinity plume of the WAC (Sellschopp and Álvarez, 2003). Changes in

salinity and the related offset in the oxygen isotope values of the surface waters impact the oxygen isotope values of the carbonates recorded in foraminifera, whereas the effect on the Mg/Ca values of foraminiferal tests is limited (Wit et al., 2010, 2013; Hönisch et al., 2013). Hence, when appreciable changes in salinity occur, temperature reconstructions based on oxygen isotopes do not exclusively reflect the seasonal SST range (Grauel and Bernasconi, 2010; Wit et al., 2010). Such a combined temperature and salinity influence on the $\delta^{18}\text{O}$ recorded may be reflected in the observed multiple maxima and calculated non-normal distribution of values at some intervals studied here (Table 2; Fig. 4c).

The average carbon isotope values of single *G. ruber* (white) specimen are similar to those found for the bulk *G. ruber* (white) samples during the last 3500 years for most of the selected time intervals, except during the RHP and the MCA (Figs. 4a and 5b). During these specific intervals the limited number of available specimens resulted in analysis of a set of additional, larger individuals (355–500 μm). The observed offset ($\pm 0.5\text{‰}$) is in line with previous studies showing ontogenetic impact on carbon isotopic fractionation (Erez and Honjo, 1981; Elderfield et al., 2002; Diz et al., 2012). The impact on oxygen isotopes over the same size range is negligible (e.g., Diz et al., 2012). Comparing oxygen isotope values derived from analysis on combined specimen for the downcore record to average values based on the individual specimen analysis shows a major offset during the RHP, and minor offsets during the LIA and the present interval (Table 1). Because the pooled samples

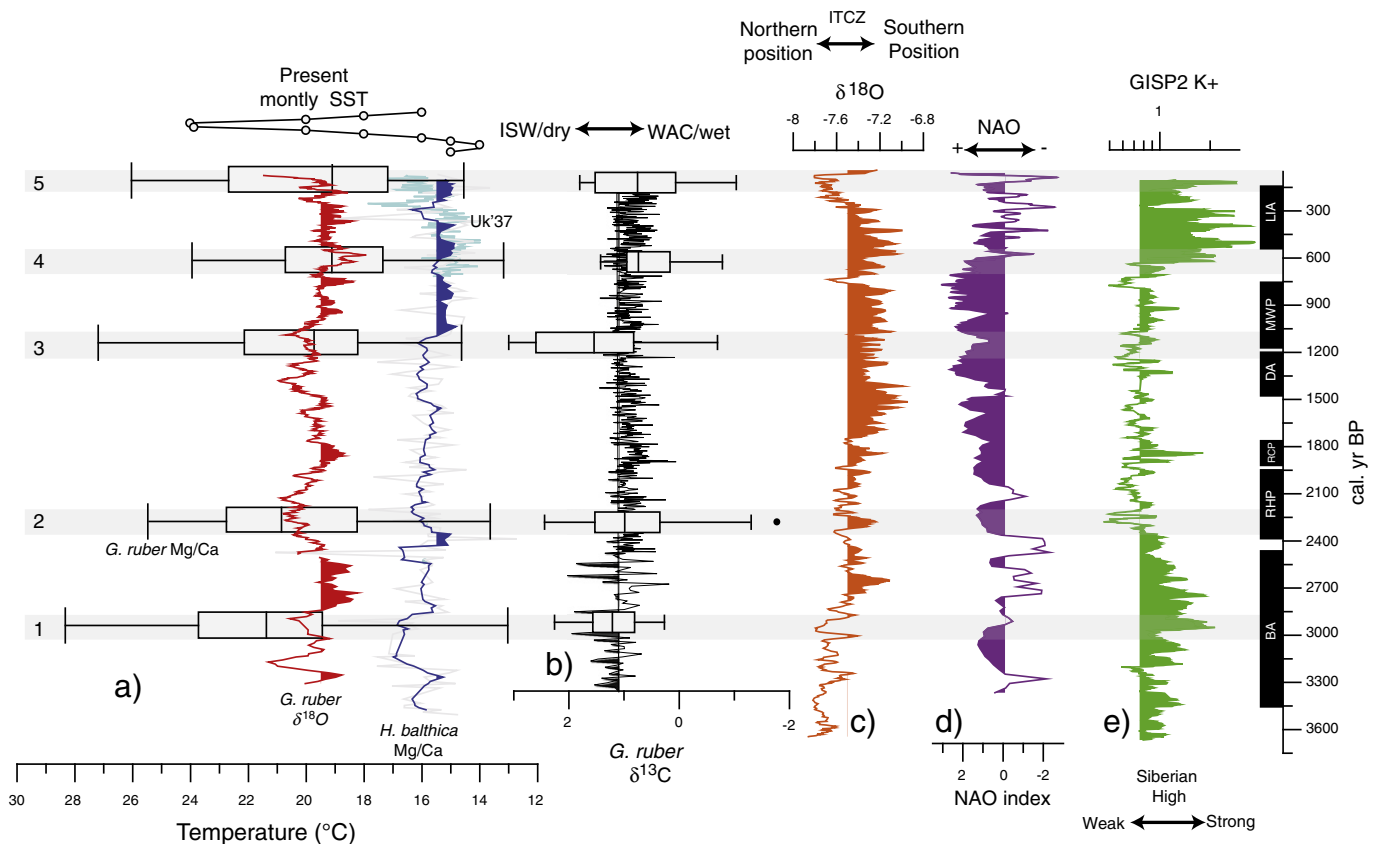


Fig. 5. (a) SST based on Mg/Ca of single specimens of *G. ruber* (white) (box-whisker plots, this study), $\delta^{18}\text{O}$ of *G. ruber* (white) (red line, Grauel et al., 2013a,b; 0–2000 years BP) and this study (2000 years BP–3400 years BP) and BWT based on Mg/Ca of *H. balthica* (dark blue line, this study) and U^{37} (light blue line, Versteegh et al., 2007). (b) $\delta^{13}\text{C}$ of individual specimens of *G. ruber* (white) from the selected time intervals (box-whisker plots, this study) and $\delta^{13}\text{C}$ of *G. ruber* (white) from bulk samples (Grauel et al., 2013b; 0–2000 years BP) and this study (2000 years BP–3400 years BP). (c) Reconstruction of the strength of the ITCZ based on an oxygen isotope record from a stalagmite from the Dongge Cave. (d) A reconstruction of the NAO index based on geochemical data from a lake in Greenland (Olsen et al., 2012) and the difference between ... records from Scotland and Morocco (Trouet et al., 2009). (e) Potassium content of the GISP2 ice core, reflecting the Siberian High (Mayewski et al., 1997). Box-whisker plots summarize the variability in the data. The caps at the end of each box indicate the extreme values (minimum and maximum), boundaries of the box are defined by the lower and upper quartiles, and the line in the center of the box is the median. Outliers beyond the extreme values are indicated with black dots. The boundary between the filled and not filled interval for the continuous proxy records indicate present day values of the different proxies used. Dark rectangles correspond to various periods mentioned in the text: Bronze Age (BA, Mayewski et al., 2004), Roman Humid Period (RHP), Roman Classical Period (RCP), Dark Ages (DA), Medieval Climate Anomaly (MCA) and Little Ice Age (LIA) as defined by Grauel et al. (2013b). Gray bars reflect the interval selected for individual *G. ruber* (white) test chemistry as in Fig. 1c and Table 1.

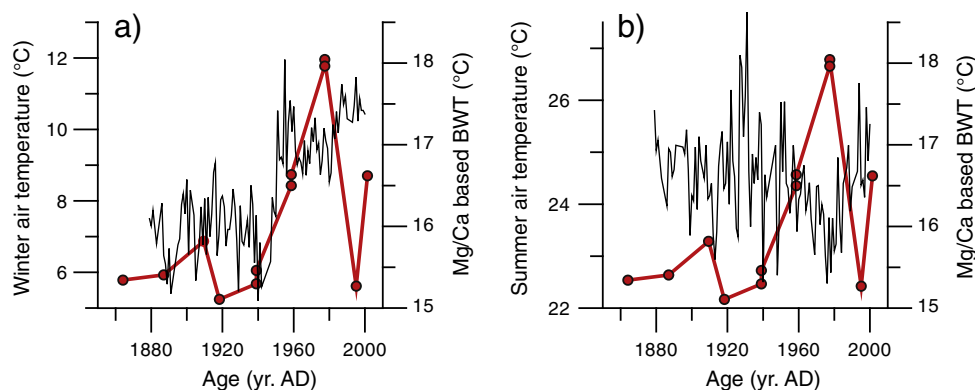


Fig. 6. *H. balthica* Mg/Ca derived bottom water temperature using the non-linear equation by Rosenthal et al. (2011) of core NU 04 (red line) compared to Italian winter (a) and summer (b) measured air temperatures; based on a combination of historical records from a variety of Italian cities as found in the National Climate Data Centre (<http://www.ncdc.noaa.gov/oa/pub/data/ghcn/v2/ghcnftp.html>); by Versteegh et al., 2007, black line). Please note that the data is presented in year AD to simplify the comparison with this recent data set.

consisted of 20 specimens, the obtained values integrate intra-annual variability. The standard error observed during the RHP (~ 0.33) is relatively high compared to the standard error based on the individual species analysis (0.5). This suggests that inter-annual variability played a major role during the RHP. Since the down-core record best integrates intra- and inter-annual variability, averages based on the down-core isotope records are used for the selected intervals. These averages are also statistically more robust, as they generally include over 200 specimens per interval. Although the average carbon isotopes of the single measured *G. ruber* (white) differ from the pooled downcore record, its variance may still be used to reconstructed actual variance during these intervals.

The Bartlett's and Kruskal–Wallis tests indicate that the variance of carbon isotopes is significantly different between the various time slices (Table 2). Grauel and Bernasconi (2010) observed strong variability in *G. ruber* (white) carbon isotopes in surface sediment samples from the south-western Adriatic and Gulf of Taranto. They related the high variance to the strong nutrient gradient between the eutrophic waters from the WAC and the more oligotrophic ISW. When the WAC dominates, the nutrient regime in the Gulf of Taranto promotes abundance of *G. ruber* (white) in the upper 5 m, while it lives deeper (~ 30 – 50 m) during periods when the influence of the WAC is reduced. Such a shift affects severely the carbon isotope chemistry in the shell of *G. ruber* (white) as it induces a change in symbiont activity, one of the main factors controlling carbon isotope values of foraminiferal test (Spero and Williams, 1989; Spero, 1992). Therefore, the range observed in $\delta^{13}\text{C}$ of individual specimens of *G. ruber* (white) of each sample is a potential representation of variance for the influence of the WAC in the study area. It should be taken into account that differences in the depth habitat of *G. ruber* (white) also affect SST reconstructions as deeper waters are colder. This could potentially also affect the temperature reconstructions made. However, although SSTs of the upper 30 m vary greatly over the year ($\Delta = 12^\circ\text{C}$), temperature variability is much lower within the upper 30 m of the water column during a single month (maximally $\Delta = 4^\circ\text{C}$; Fig. 1d). Furthermore, no significant correlation is observed between individual specimen Mg/Ca ratios and $\delta^{13}\text{C}$ values (Fig. 3b). This suggests that changes in reconstructed temperatures due to differences in calcification depth of *G. ruber* (white) are minimal.

The carbon isotopes of tests of *G. ruber* (white) from core tops in the Gulf of Taranto and South Adriatic range from 0 to 2‰ (Grauel and Bernasconi, 2010), closely corresponding to the observed range for the individual *G. ruber* (white) $\delta^{13}\text{C}$ from the 'present-day' interval of core DP30 (Fig. 4a). The other intervals show a somewhat larger range in *G. ruber* (white) $\delta^{13}\text{C}$ values. Because average values of *G. ruber* (white) test geochemistry are biased towards summer conditions and the WAC is reduced during summer, the average $\delta^{13}\text{C}$ of *G. ruber* (white) should be enriched as well. Therefore, we suggest that the

lower values (-1 to 0‰) in the most recent sample represent individuals from winter/spring season, when WAC impact is higher.

Since the variability in *G. ruber* (white) Mg/Ca-based SSTs appears to represent seasonality in the Gulf of Taranto, differences in the observed range should reflect changes in seasonality. Although there appear trends in the SST variance, and therefore seasonality, the performed Bartlett's test shows no significant changes in Mg/Ca between the different intervals (Table 2). Nevertheless, trends may be verified by comparing the ranges with those of other down-core temperature reconstructions.

5.1.2. Reconstructing summer conditions: bulk *G. ruber* (white) test chemistry

Because the bulk oxygen and carbon isotopes of *G. ruber* (white) are skewed towards the warm and more oligotrophic summer season in the Gulf of Taranto, bulk oxygen isotope values of *G. ruber* (white) can potentially be used to reconstruct variability in average summer temperature. However, oxygen isotope based temperatures are also impacted by changes in $\delta^{18}\text{O}_w$. Still, the average Mg/Ca of single specimens of *G. ruber* (white) based temperature reconstructions and the bulk *G. ruber* (white) $\delta^{18}\text{O}$ matches for the largest part of the record, except during the BA (Fig. 5a). This suggests that in general, bulk *G. ruber* (white) $\delta^{18}\text{O}$ reflects primarily summer temperatures for this region.

For the intervals in which the Mg/Ca of *G. ruber* (white) have been measured, it is possible to compare average Mg/Ca-based temperatures with the average oxygen isotope values for the downcore foraminiferal record of the interval (Fig. 7a). Changes in sea surface salinity (SSS) can theoretically be calculated by combining oxygen isotope and Mg/Ca values. However, the range in SSSs calculated this way is much broader than is observed today. When calculating SSS from calcitic Mg/Ca and oxygen isotopes, uncertainties in both proxies and effects related to additional variables contribute to an uncertainty in the reconstructed mean value (Schmidt et al., 1999; Rohling, 2000). In addition, the relationship between $\delta^{18}\text{O}_w$ and salinity is not straightforward and might vary over time, space, and region (Schmidt et al., 1999; Rohling, 2000). Among others, oxygen isotopes of Italian winter precipitation are more depleted ($< -6\text{‰}$) than those of summer precipitation ($> -6\text{‰}$). This difference in isotopic composition of precipitation is partly due to the seasonal temperature contrast and partly to differences in the source areas of the moisture (Longinelli and Selmo, 2003). A shift in the contribution of different seasons to the overall precipitation can therefore have a large impact on the average isotopic signature of Italian precipitation (Longinelli and Selmo, 2003). Hence, variance of reconstructed SSS reflects both SSS variability through time and variability arising from analytical and calibration uncertainties. This implies that it may not be possible to accurately calculate salinities for individual specimens in this way. Nevertheless, as these errors should act upon each individual specimen in a random direction, average $\delta^{18}\text{O}_w$ values

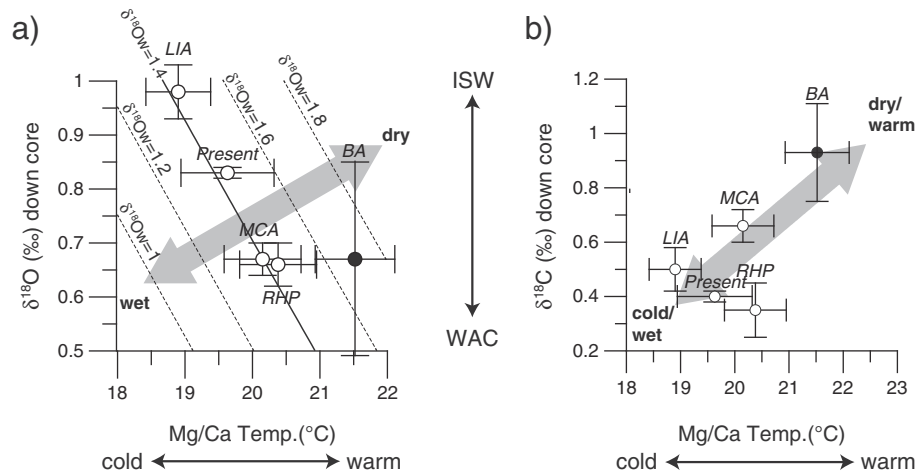


Fig. 7. Average of the SSTs based on the individual measured *G. ruber* (white) Mg/Ca versus average $\delta^{18}\text{O}$ and $\delta^{13}\text{C}$ (b) of *G. ruber* (white) from the pooled downcore data set downcore. Dashed lines in (a) represent the correlation between $\delta^{18}\text{O}$ and temperature under variations of $\delta^{18}\text{O}_w$ based on Eq. (1) (see text). Abbreviations stand for the events matching with the studied intervals (see Fig. 1c and Table 1): Bronze Age (BA, Mayewski et al., 2004) and Roman Humid Period (RHP), Roman Classical Period (RCP), Dark Ages (DA), Medieval Climate Anomaly (MCA) and Little Ice Age (LIA) as defined by Grauel et al. (2013b). ISW is ionian surface water. WAC is West Adriatic current.

could still provide a robust estimate of past (summer) SSS. This is confirmed by the good correspondence between the average of calculated present-day SSS (39.2) based on $\delta^{18}\text{O}_w$ and measured present-day SSS in the Gulf of Taranto in summer (38.9; Zonneveld et al., 2009).

Plotting iso-isotope lines in the same plot makes it possible to unravel the effect of temperature and surface water stable isotope composition ($\delta^{18}\text{O}_w$, Fig. 7a). During all intervals, except the BA, the oxygen isotopic value of the surface waters has been very close to the present-day value of 1.4‰ (Fig. 7a). During the BA, surface-water stable oxygen isotope values must have been higher, at about 1.65‰ (Fig. 7a). The higher isotopic value for the surface water during the BA is probably connected to higher surface water salinity at that time. This is confirmed when comparing these data to the downcore $\delta^{13}\text{C}$ record for *G. ruber* (white) (Fig. 5b). During the BA, $\delta^{13}\text{C}$ values are higher, reflecting a reduced influence of the WAC, hence drier overall conditions (Fig. 7b). All other intervals appear more or less similar to the present-day interval (Fig. 7b).

5.1.3. Winter conditions reflected by *H. balthica* Mg/Ca values

Mg incorporated in the tests of *H. balthica* exhibits an unusual high temperature sensitivity (Rosenthal et al., 2011), making this species ideal for bottom water temperature reconstructions (Wit et al., 2012). Although the temperature calibration for *H. balthica* by Rosenthal et al. (2011) was based on specimens collected from the Indonesian coast and the northeastern Atlantic ocean, temperatures based on the Mg/Ca values measured on *H. balthica* over the last decades ($\sim 16^\circ\text{C}$) resemble present-day bottom water temperature (14 to 15°C ; Figs. 1d, 5a and 6).

Bottom water temperatures (BWT) in the Gulf of Taranto are set during late winter/early spring when surface waters cool, resulting in convective turnover (Fig. 1d). This mixing thereby sets temperature and composition of this deep water, which is maintained until the subsequent deep winter-mixing event. Coherently, the record of reconstructed BWTs shows similar patterns as historical records of Italian winter and spring air temperatures of the last hundred years (Fig. 6a). For example, measured Italian winter air temperature as well as the reconstructed BWTs show a sharp increase in temperature around 1940 AD. Furthermore, observed maxima based on *H. balthica* Mg/Ca values during the last 800 years correspond to SST maxima and average SSTs based on the U_{37}^k from nearby cores (Versteegh et al., 2007; Grauel et al., 2013a, Fig. 5a). This is in line with our interpretation on the *H. balthica* Mg/Ca record as a winter temperature proxy as several

studies suggested that U_{37}^k in this region is strongly influenced by changes in surface water temperature during winter and early spring (Sangiorgi et al., 2003; Versteegh et al., 2007; Leider et al., 2010; Grauel et al., 2013a).

5.2. Seasonal contrast in temperature and precipitation during the last 3500 years

5.2.1. The RHP and MCA interval: similar seasonality as today

A similar range in temperatures ($\Delta T = \sim 10^\circ\text{C}$) is observed for present-day conditions, MCA and RHP. For the RHP the median of the Mg/Ca-based temperatures as well as the bulk *G. ruber* (white) oxygen isotopes indicate relatively warm summers compared to present-day (Figs. 4 and 5a), whereas winter conditions were probably slightly colder (Fig. 5a). Although the higher summer SST may be partly related to a shallower and thus warmer habitat of *G. ruber* (white) during a humid summer season, somewhat higher summer SSTs are in line with a reconstruction based on dinoflagellate cysts from the same core during the latest part of the RHP and the beginning of the Roman Classical Period (2010 cal. years BP–1860 cal. years BP; Chen et al., 2011). Several other studies also inferred overall warm conditions across southern Europe during the RHP (e.g., Desprat et al., 2003; Holzhauser et al., 2005; Martín-Chivelet et al., 2011). Nonetheless, overall seasonal contrast during the RHP was similar to that of the present-day.

During the early MCA (~ 1000 cal. years BP) mild winters and warm summers, similar as today, are observed based on the *H. balthica* Mg/Ca and individually measured *G. ruber* (white) Mg/Ca values, respectively (Fig. 5a). Mild winter conditions are coherent with a variety of other reconstructions from the area (e.g., Rohling et al., 2002; Frisia et al., 2005) and might be linked to a weak Siberian high (Mayewski et al., 1997; Fig. 5e). However, for the latest part of the MCA (750–950 cal. years BP) SSTs based on Mg/Ca from *H. balthica* and on $\delta^{18}\text{O}$ from *G. ruber* (white) indicate a swift transition to colder conditions during both winter and summer that is also observed in dinoflagellate cyst-based SSTs from the same core suggesting lower SSTs during this interval (Chen et al., 2013). High primary productivity (PP) in the study area is reconstructed for the early MCA (Goudeau, 2014), which could result in shallower and thus warmer habitat of *G. ruber* (white). However, a warm early MCA (~ 1000 cal. years BP) and colder conditions during the late MCA (750–950 cal. years BP) are found across the Mediterranean

(Pla and Catalan, 2005; Frisia et al., 2006) and in the Southern Alps (Frisia et al., 2005; Holzhauser et al., 2005; Giraudi, 2009). This interval also corresponds with a transition from dry conditions to more humid conditions in the western Mediterranean (Nieto-Moreno et al., 2013b). This suggests that this transition is related to shifts in atmospheric patterns, as the transition is not restricted to temperature variability but also includes changes in precipitation patterns. Colder summer conditions align with a more southward position of the ITCZ inferred from a speleotherm $\delta^{18}\text{O}$ record (Wang et al., 2005; Fig. 5c). The colder winter temperatures are, however, more difficult to explain as the Siberian high appears relatively weak compared to RCC events as the LIA and BA (Fig. 5e). A recent study on ice-rafted debris, however, has suggested that a negative Arctic Oscillation (AO) persisted between 1150 and 150 cal. years BP (Darby et al., 2012). The latter could enhance the potential outbreaks of cold polar air across the study area during winter (Rohling et al., 2002).

The reconstructed similarity in humidity for the present, MCA and RHP as reflected in the inferred $\delta^{18}\text{O}_w$ of 1.4‰ (Fig. 7a) is confirmed not only by the average of the pooled $\delta^{13}\text{C}$ of *G. ruber* (white) but also by similar variability in the individual $\delta^{13}\text{C}$ of *G. ruber* (white) during these intervals (Fig. 5b). In contrast, variance during LIA and BA is smaller, albeit with averages that are not similar. The high variance during present-day, MCA and RHP suggests a high seasonal contrast in precipitation, which is also typical for the present-day Mediterranean climate (Fig. 4b). Down-core $\delta^{18}\text{O}$ combined with Mg/Ca of *G. ruber* results in similar $\delta^{18}\text{O}_w$ values as today (1.4‰, Fig. 7a), suggesting that summers were as dry as today. This, in combination with a similar variability in single specimen $\delta^{13}\text{C}$ of *G. ruber* (white), implies that winter precipitation has remained the main source for moisture during the RHP and MCA. However, the average $\delta^{13}\text{C}$ of the pooled *G. ruber* (white) suggests that summer conditions were slightly more humid during the RHP and drier during the MCA (Grauel et al., 2013b).

General consensus on the relatively humid nature of the RHP is that these conditions are related to a negative state of the NAO (e.g., Giraudi et al., 2011; Nieto-Moreno et al., 2011; Dermody et al., 2012). However, during this interval also a centennial scale southward displacement of the subtropical high-pressure cell is found (Fig. 5c, Fleitmann et al., 2003; Wang et al., 2005; Shanahan et al., 2009) which would allow the westerlies to enter the study area also in summer. The observed range in $\delta^{13}\text{C}$ is similar to the recent range suggesting a similar range in precipitation as today. This indicates that either winter precipitation was also increased, or that summer was the most humid season during this period. The latter seems more plausible as the interval studied here is coherent with a centennial shift to a relatively positive NAO (Olsen et al., 2012). In contrast, the calculated $\delta^{18}\text{O}_w$ (~1.4‰) is not in line with more humid summer conditions during the RHP. However, this may be due to the less depleted $\delta^{18}\text{O}_w$ of summer precipitation (>−6‰) compared to winter precipitation (<−6‰). In addition, during the sampled time interval inter-annual variability appeared to be large (see discussion above), which could have biased our calculated $\delta^{18}\text{O}_w$.

Besides a centennial scale event, the interval corresponding to the MCA is predominantly characterized by a relatively positive mode of NAO (Olsen et al., 2012; Fig. 5d). Under persistent positive NAO conditions, the westerlies reach a larger area and extend more southwards than normally, likely including the Alps. This may have affected drainage by the river Po and increased run-off by rivers located in Northern Italy (Magny et al., 2013; Peyron et al., 2013). Such a contrast in humid/arid conditions between northern and southern Italy during other RCC events, such as the 4.2 kyr event, was demonstrated on the basis of Italian lake deposits (e.g., Magny et al., 2003; Joannin et al., 2012; Magny et al., 2013; Peyron et al., 2013). Increased run-off from more northern sources during the MCA period is also evident from the contrasting patterns found in cores taken in the Northern Adriatic (Piva et al., 2008) and the Southern Adriatic Sea (Siani et al., 2013). Under such conditions the associated excess rain would enhance Po River outflow. As the Po River contributes up to 70% of all river water input to the Adriatic Sea (Raicich, 1996), this would severely increase

the WAC, reducing salinity in the Gulf of Taranto. Such an increased WAC in winter is in line with the observed depleted $\delta^{13}\text{C}$ values during the MCA (Figs. 4b, 5b), while the enriched $\delta^{13}\text{C}$ values can be related to a dry summer season.

5.2.2. The LIA: cold and humid conditions year round

Cold winter conditions are reconstructed for the early LIA, inferred from the BWT based on Mg/Ca from *H. balthica* (Fig. 5a). The GISP2 K^+ indicates that during the LIA, Bora winds might have increased (Fig. 5e), as they are closely linked to the Siberian high (Mayewski et al., 1997). This is in line with Rohling et al. (2002) suggesting that cold Bora winds are responsible for winter cooling in the Mediterranean area during other RCC-events such as the 8.2 kyr event. In addition to the colder winters, summer temperatures were also lower (~19–24 °C) during the LIA (Fig. 4b,c and 5a). This indicates that cool conditions persisted year-round, which is consistent with results of SST reconstructions based on $\text{TEX}^{\text{H}}_{86}$ (assumed to reflect summer temperatures) and U^{K}_{37} (assumed to reflect winter/spring conditions) from the same area (Versteegh et al., 2007; Grauel et al., 2013a). These year-round cold conditions are accompanied by a similar seasonality as today ($\Delta T = \sim 10^\circ\text{C}$, Fig. 1c). During the late LIA (305–235 cal. years BP), however, a higher seasonal contrast may have existed (e.g., Grove, 2001; Nicault et al., 2008; Grauel et al., 2013a). Low BWTs based on Mg/Ca from *H. balthica* and high SSTs based on $\delta^{18}\text{O}$ of *G. ruber* (white), confirm a relatively high seasonal contrast for the late LIA (Fig. 5a).

The individually measured *G. ruber* (white) $\delta^{13}\text{C}$ values show a relatively small range during the LIA, also when compared to present-day core top data (Figs. 4b and 5b). The range in $\delta^{13}\text{C}$ is primarily controlled by changes in WAC inflow during the year. The observed limited range and overall depleted values, therefore, suggest prolonged inflow of the relatively low-saline WAC over the year as also suggested by Grauel et al. (2013a). Hence, summers would be relatively humid in addition to the already typically humid winters. Because the oxygen isotopes for summer precipitation are less depleted than those for winter precipitation, this may not be reflected in the average oxygen isotope value of the surface water (Fig. 7a). Relatively humid winters and summers are coherent with patterns found in cores from the north Adriatic Sea and Italian lakes (Piva et al., 2008; Giraudi et al., 2011). Furthermore, during the LIA, the more southern position of the Hadley cell (cf. Wang et al., 2005) would allow the westerlies to enter the Mediterranean area also during summer. Thus the overall relatively humid and cool LIA period in the central Mediterranean, as reflected in our results, is consistent with observations made in records elsewhere (Piva et al., 2008; Grauel et al., 2013a; Nieto-Moreno 2013a,b). It should be noted that under the influence an increased WAC in summer, *G. ruber* (white) may live in shallower and warmer waters, and therefore, actual summer SSTs could have been slightly lower than those recorded by our proxies.

5.2.3. The Bronze Age: cold, dry winters and warm, dry summers

The BA is the only episode in our record during which both temperature and salinity deviate considerably from the other intervals (Figs. 5a, 7a). Summer temperatures were high, apparent from both $\delta^{18}\text{O}$ and Mg/Ca values of *G. ruber* (white; Fig. 5a). Dry summer conditions, allows *G. ruber* (white) to live in deeper and colder water depths which could affect our summer SST reconstruction. Actual summer SST thus may have been somewhat higher than the reconstructed SST. Although *G. ruber* (white) habitat changes under the influence of the WAC, it is also known to have a preference for relatively low-salinity waters (Rohling et al., 2004). Therefore, we assume that the deepening of its habitat, resulting in lower reconstructed summer SSTs, was relatively restricted during this extremely dry interval compared to present-day migration of *G. ruber* (white). Warm and dry summers are consistent with a relatively northward summer position of the ITCZ at that time (Fleitmann et al., 2003; Wang et al., 2005; Weldeab et al., 2007; Table 1, Fig. 5c). Increased summer temperatures are in

line with pollen records from Greek and Italian lakes (e.g., Peyron et al., 2011). The large range of reconstructed temperatures (13–28 °C) from Mg/Ca measured on single specimens of *G. ruber* (white) suggests that warm summers were accompanied by cold winters (Fig. 5a).

The GISP2 K^+ indicates a relatively strong Siberian high and possibly related increased strong Bora winds during winter (Mayewski et al., 1997; Rohling et al., 2002, Fig. 5e). This period is coherent with the timing of one of the RCC-events as indicated by Mayewski et al. (2004). Cold outbreaks associated with this RCC-event would explain the inferred low winter temperatures (reduced by 2 °C compared to the most recent time slice). In general, these RCC-events are mostly related to changes in northern hemisphere high-latitude winter conditions (Denton et al., 2005; Wanner et al., 2011). Decreased winter/early spring temperatures are also suggested by $U^{K_{37}}$ from a core in the southern Adriatic Sea (Sangiorgi et al., 2003). In contrast, our *H. balthica* Mg/Ca record indicates higher BWT, suggesting increased winter temperatures. However, as discussed above, the surface waters were possibly much more saline during this period (Fig. 7a), which in turn, would require less cooling to descend to the same depth. In addition, the outbreaks of polar air over the Adriatic Sea would enhance the formation of nADW and sADW, contributing to a more ventilated and less stratified water column for a longer period during the year. This adequately explains the observed apparent discrepancy between temperatures based on Mg/Ca from specimens of *H. balthica* and the other winter temperature records. Furthermore it emphasizes that changes in oceanography should be taken into account when interpreting paleo-temperature records in this area (Grauel et al., 2013a).

Dry conditions, responsible for the enriched $\delta^{18}O_{wv}$, are reflected in a lower impact of the WAC in the Gulf of Taranto, evidenced by relatively high $\delta^{13}C$ values of *G. ruber* (bulk) (Figs. 5b, 7b). Furthermore, the lowest range in the individually measured *G. ruber* (white) $\delta^{13}C$ values is observed during the BA (Figs. 5b and 4a). Such a narrow range implies that both summer and winter precipitation was modest. A relatively positive mode of the NAO during this period (Olsen et al., 2012, Fig. 6d), in combination with cold, dry Bora winds (Rohling et al., 2002; Fig. 6e) would reduce winter precipitation. A relative northward position of the ITCZ in summer would have resulted in arid summers (Fig. 5d). Similar year-round low precipitation during the BA in central Italy was suggested by Peyron et al. (2011), in coherence with other records across the Mediterranean (Bar-Matthews et al., 2003; Di Rita and Magri, 2009; Kaniewski et al., 2010; Giraudi et al., 2011; Nieto-Moreno et al., 2011; Combourieu-Nebout et al., 2013; Goudeau et al., 2014). Reconstructed SSTs based on $U^{K_{37}}$ (Sangiorgi et al., 2003) and the test chemistry of *G. ruber* (white) both suggest that these conditions may have persisted from 2850 to 3150 cal. years BP (Fig. 5a, b). During the Late BA several cities and states in the Eastern Mediterranean region were distorted, such as the Mycenaean civilization (e.g., Carpenter, 1966; Weiss, 1982). This has been related to severe drought (Carpenter, 1966; Weiss, 1982). The reconstruction presented here illustrates that during the BA summers were warm and winters cold, but aridity lasted year-round. This must have had a profound impact on early agriculture, also in Southern Italy.

5.3. Changing climatic patterns over the Mediterranean and seasonality

Although seasonality remained relatively constant throughout the intervals studied here, comparison with other proxies reveals that during the BA and the LIA winter conditions were relatively cold. This is in coherence with earlier work by Denton et al. (2005) and Rohling et al. (2002), who suggested that millennial scale cold events in the northern hemisphere were mainly related to winter climate. These changes in northern hemisphere winter climate were suggested to also affect the position of the ITCZ during summer (Denton et al., 2005). Mediterranean summer climate is closely coupled to the ITCZ position as the descending limb of the northern Hadley cell is responsible for the strong high pressure cell over the Mediterranean during summer. This high

pressure cell effectively blocks the Mediterranean from the influence of the westerlies. The contrasting seasonality between the BA (high variance) and the LIA (low variance) suggests that the connection between high- and low-latitude climate variability did not remain stable through time.

Comparing the $\delta^{13}C$ values of single *G. ruber* (white) tests indicates that the seasonal contrast in precipitation in the Central Mediterranean did not remain constant over the last 3500 years (Figs. 4b, 5a). Differences in the ITCZ position during summer and the NAO state during winter together control changes in the seasonal contrast in Mediterranean precipitation. The high intra-annual variability inferred for the RHP and MCA contrasts with the low intra-annual variability during LIA and BA. Decoupled changes in winter and summer precipitation imply that ITCZ and NAO variability are not necessarily linked directly.

Nonetheless, a relation between temperature/precipitation and seasonality is apparent from the trend between average $\delta^{13}C$ and the SSTs based on Mg/Ca from *G. ruber* (white) (Fig. 7b), a pattern confirmed by $\delta^{18}O_{wv}$ inferred from combining $\delta^{18}O$ and the Mg/Ca SST reconstructions of *G. ruber* (white). The trend observed between the different intervals studied here suggests that when warmer conditions prevail, it is also dryer, while it is moister during colder conditions. These observations are in agreement with the sub-tropical, Mediterranean setting: Warm and dry conditions characterize summers, while humid and cold conditions prevail during winter. Although the seasonal temperature contrast remained similar across the studied RCC intervals, the precipitation balance was dramatically different between the LIA and the BA. During the LIA humid and cold, winter-like conditions dominated, whereas during the BA dry conditions prevailed throughout the year.

6. Conclusions

Variance in Mg/Ca and $\delta^{13}C$ of the single specimen measurements on *G. ruber* (white) reflect the present-day range of Gulf of Taranto sea surface temperatures and precipitation respectively, albeit with their averages biased towards summer conditions. Reconstructions based on the measured individual test chemistry indicate that temperature contrast did not change significantly during the last 3500 years. However, comparing overall patterns with other proxies for winter and summer SSTs in the Gulf of Taranto, there are appreciable differences. Present-day bottom water temperature (BWT) in the Gulf of Taranto is set in winter. Hence, reconstructed BWT based on *H. balthica* Mg/Ca reflects SST-patterns for winter/spring (SSTw). This SSTw concurs with the previously reconstructed SST based on $U^{K_{37}}$ (a winter/spring proxy). Summer SSTs can be reconstructed using pooled *G. ruber* (white) test chemistry as a proxy. Our data suggest that winters are cool during Rapid Climate Change events, such as the BA and LIA, compared to other intervals. However, results from our proxies also indicate that during the early LIA summers are cold and wet, whereas during the BA interval summer conditions are warm and dry. Furthermore, reconstructed humidity suggests year-round aridity during the BA interval, while the LIA interval is characterized by relatively humid conditions throughout the year. The trend observed between average carbon isotopes and SST based on Mg/Ca *G. ruber* (white), reflecting precipitation and temperature respectively, indicates that the LIA is characterized by more 'winter'-like conditions (cold and wet), while the BA is more skewed to 'summer'-like conditions (warm and dry). The other RCC-periods (MCA and RHP) are characterized by intermediate seasonal contrast similar to today. Summer conditions are controlled by low-latitude climate forcing (e.g. ITCZ) and winter climate by high-latitude climate variability (NAO, Siberian High). The contrasting patterns during the LIA and BA suggest that connections between high and low latitude climate variability are not necessarily continuous during RCC events.

Acknowledgments

We thank H. de Waard at Utrecht University, for lab assistance with LA-ICP-MS; W. Boer at the NIOZ, for lab assistance with ICP-MS and S.E. Bishop and M. Coray-Strasser at ETH, for lab assistance. We are grateful to the captain and crew, and to all participants on board the DOPPIO cruise with R.V. Pelagia (coordinated by G. J. De Lange) for the sample collection and for the help during the sub-sampling of DP30 by A. Leider and C.E. Casalino.

This work was supported by the Dutch Science Foundation (NWO) and the SNF (Swiss National Science Foundation Project 20MA21-115934) as part of the MOCCHA-project initiated by the European Science Foundation (ESF) Eurocores Programme EuroMARC.

References

- Alpert, P., Baldi, M., Ilani, R., Krichak, S., Price, C., Rodó, X., Saaroni, H., Ziv, B., Kishcha, P., Barkan, J., Mariotti, A., Xoplaki, E., 2006. Chapter 2: relations between climate variability in the Mediterranean region and the tropics: ENSO, South Asian and African monsoons, hurricanes and Saharan dust. In: Lionello, P., P.M.R., Boscolo, R. (Eds.), *Developments in Earth and Environmental Sciences*. Elsevier, pp. 149–177.
- Anand, P., Elderfield, H., Conte, M.H., 2003. Calibration of Mg/Ca thermometry in planktonic foraminifera from a sediment trap time series. *Paleoceanography* 18 (2), 1050.
- Bárcena, M.A., Flores, J.A., Sierro, F.J., Pérez-Folgado, M., Fabres, J., Calafat, A., Canals, M., 2004. Planktonic response to main oceanographic changes in the Alboran sea (Western Mediterranean) as documented in sediment traps and surface sediments. *Mar. Micropaleontol.* 53 (3), 423–445.
- Bar-Matthews, M., Ayalon, A., Gilmour, M., Matthews, M., Hawkesworth, C., 2003. Sea-land isotopic relationships from planktonic foraminifera and speleothems in the Eastern Mediterranean region and their implications for paleorainfall during interglacial intervals. *Geochim. Cosmochim. Acta* 67, 3181–3199.
- Boer, W., Van den Bergh, G., De Haas, H., De Stigter, H., Gieles, R., Van Weering, T., 2006. Validation of accumulation rates in Teluk Banten (Indonesia) from commonly applied ^{210}Pb models, using the 1883 Krakatau tephra as time marker. *Mar. Geol.* 227 (3), 263–277.
- Boyle, E.A., Keigwin, L.D., 1985. Comparison of Atlantic and Pacific paleochemical records for the last 215,000 years: changes in deep ocean circulation and chemical inventories. *Earth Planet. Sci. Lett.* 76 (1–2), 135–150 (12).
- Brandimarte, L., Di Baldassarre, G., Bruni, G., D'Odorico, P., Montanari, A., 2011. Relation between the north-Atlantic oscillation and hydroclimatic conditions in Mediterranean areas. *Water Resour. Manag.* 25, 1269–1279.
- Bronk Ramsey, C., Higham, T.F.G., Brock, F., Baker, D., Ditchfield, P., 2009. Radiocarbon dates from the Oxford AMS system: archaeometry datelist 33. *Archaeometry* 51, 323–349.
- Büntgen, U., Tegel, W., Nicolussi, K., McCormick, M., Frank, D., Trouet, V., Kaplan, J.O., Herzog, F., Heussner, K.U., Wanner, H., 2011. 2500 years of European climate variability and human susceptibility. *Science* 331 (6017), 578–582.
- Carpenter, R., 1966. *Discontinuity in Greek Civilization*. Cambridge University Press, Cambridge.
- Chen, L., Zonneveld, K.A.F., Versteegh, G.J.M., 2011. Short term climate variability during “Roman classical period” in the Eastern Mediterranean. *Quat. Sci. Rev.* 30, 3880–3891.
- Chen, L., Zonneveld, K.A.F., Versteegh, G.J.M., 2013. Paleoclimate of the southern Adriatic Sea region during the “Medieval Climate Anomaly” reflected by organic walled dinoflagellate cysts. *The Holocene* 23, 645–655.
- Cini Castagnoli, G., Bonino, G., Caprioglio, F., Provenzale, A., Serio, M., Guang, Mei, Zh., 1990. The carbonate profile of two recent Italian sea cores: evidence that the sedimentation rate is constant over the last millennia. *Geophys. Res. Lett.* 17 (11), 1937–1940.
- Combouret-Nebout, N., Peyron, O., Bout-Roumazielles, V., Goring, S., Dormoy, I., Joannin, S., Sadori, L., Siani, G., Magny, M., 2013. Holocene vegetation and climate changes in the Central Mediterranean inferred from a high-resolution marine pollen record (Adriatic Sea). *Clim. Past* 9 (5), 2023–2042.
- Darby, D.A., Ortiz, J.D., Grosch, C.E., Lund, S.P., 2012. 1,500-year cycle in the Arctic oscillation identified in Holocene Arctic sea-ice drift. *Nat. Geosci.* 5, 897–900.
- Denton, G.H., Alley, R.B., Comer, G.C., Broecker, W.S., 2005. The role of seasonality in abrupt climate change. *Quat. Sci. Rev.* 24, 1159–1182.
- Dermody, B.J., de Boer, H.J., Bierkens, M.F.P., Weber, S.L., Wassen, M.J., Dekker, S.C., 2012. A seesaw in Mediterranean precipitation during the Roman period linked to millennial-scale changes in the north Atlantic. *Clim. Past* 8 (2), 637–651.
- Desprat, S., Sánchez-Gómez, M.F., Loutre, M.F., 2003. Revealing climatic variability of the last three millennia in northwestern Iberia using pollen influx data. *Earth Planet. Sci. Lett.* 213 (1), 63–78.
- Di Rita, F., Magri, D., 2009. Holocene drought, deforestation and evergreen vegetation development in the Central Mediterranean: a 5500 year record from Lago Alimini Piccolo, Apulia, southeast Italy. *The Holocene* 19 (2), 295–306.
- Dissard, D., Nehrkke, G., Reichert, G.J., Bijma, J., 2010. The impact of salinity on the Mg/Ca and Sr/Ca ratio in the benthic foraminifera *Ammonia tepida*: results from culture experiments. *Geochim. Cosmochim. Acta* 74 (3), 928–940.
- Diz, P., Barras, C., Geslin, E., Reichert, G.J., Metzger, E., Jorissen, F., Bijma, J., 2012. Incorporation of Mg and Sr and oxygen and carbon stable isotope fractionation in cultured *Ammonia tepida*. *Mar. Micropaleontol.* 92, 16–28.
- Dueñas-Bohórquez, A., da Rocha, R.E., Kuroyanagi, A., Bijma, J., Reichert, G.J., 2009. Effect of salinity and seawater calcite saturation state on Mg and Sr incorporation in cultured planktonic foraminifera. *Mar. Micropaleontol.* 73 (3), 178–189.
- Dueñas-Bohórquez, A., Raitzsch, M., de Nooijer, L.J., Reichert, G.J., 2011. Independent impacts of calcium and carbonate ion concentration on Mg and Sr incorporation in cultured benthic foraminifera. *Mar. Micropaleontol.* 81 (3), 122–130.
- Elderfield, H., Ganssen, G., 2000. Past temperature and $\delta^{18}\text{O}$ of surface ocean waters inferred from foraminiferal Mg/Ca ratios. *Nature* 405 (6785), 442–445.
- Elderfield, H., Vautravers, M., Cooper, M., 2002. The relationship between shell size and Mg/Ca, Sr/Ca, $\delta^{18}\text{O}$, and $\delta^{13}\text{C}$ of species of planktonic foraminifera. *Geochim. Geophys. Geosyst.* 3 (8), 1–13.
- Erez, J., Honjo, S., 1981. Comparison of isotopic composition of planktonic foraminifera in plankton tows, sediment traps and sediments. *Palaeogeogr. Palaeoclimatol. Palaeoecol.* 33 (1), 129–156.
- Fleitmann, D., Burns, S.J., Mudelsee, M., Neff, U., Kramers, J., Mangini, A., Matter, A., 2003. Holocene forcing of the Indian monsoon recorded in a stalagmite from southern Oman. *Science* 300 (5626), 1737–1739.
- Frisia, S., Borsato, A., Spötl, C., Villa, I.M., Cucchi, F., 2005. Climate variability in the SE alps of Italy over the past 17 000 years reconstructed from a stalagmite record. *Boreas* 34 (4), 445–455.
- Frisia, S., Borsato, A., Mangini, A., Spötl, C., Madonia, G., Sauro, U., 2006. Holocene climate variability in Sicily from a discontinuous stalagmite record and the mesolithic to neolithic transition. *Quat. Res.* 66 (3), 388–400.
- Giraudi, C., 2009. Late Holocene glacial and periglacial evolution in the upper Orco Valley, northwestern Italian Alps. *Quat. Res.* 71, 1–8.
- Giraudi, C., Magny, M., Zanchetta, G., Drysdale, R.N., 2011. The Holocene climatic evolution of Mediterranean Italy: a review of the continental geological data. *The Holocene* 21 (1), 105–115.
- Goudeau, M.-L.S., 2014. Decadal to millennial time scale climate variability in the Central Mediterranean during the Holocene. A reconstruction Based on Geochemical Proxies From High Resolution Sedimentary Records/USES series 56 (Thesis).
- Goudeau, M.-L.S., Grauel, A.L., Bernasconi, S.M., de Lange, G.J., 2013. Provenance of surface sediments along the southeastern Adriatic coast off Italy: an overview. *Estuar. Coast. Shelf Sci.* 134, 45–56.
- Goudeau, M.-L.S., Grauel, A.L., Tessarolo, C., Leider, A., Chen, L., Bernasconi, S.M., Versteegh, G. J.M., Zonneveld, K.A.F., Boer, W., Alonso-Hernandez, C.M., De Lange, G.J., 2014. The Glacial-Interglacial transition and Holocene environmental changes in sediments from the Gulf of Taranto, Central Mediterranean. *Mar. Geol.* 348, 88–102.
- Grauel, A.L., Bernasconi, S.M., 2010. Core-top calibration of $\delta^{18}\text{O}$ and $\delta^{13}\text{C}$ of *G. ruber* (white) and *U. mediterranea* along the southern Adriatic coast of Italy. *Mar. Micropaleontol.* 77 (3–4), 175–186 (12).
- Grauel, A.L., Leider, A., Goudeau, M.S., Müller, I.A., Bernasconi, S.M., Hinrichs, K.U., de Lange, G.J., Zonneveld, K.A.F., Versteegh, G.J.M., 2013a. What do SST proxies really tell us? A high-resolution multiproxy ($\text{U}^{\text{K}'}_{37}$, $\text{TEX}^{\text{H}}_{86}$ and foraminifera $\delta^{18}\text{O}$) study in the Gulf of Taranto, Central Mediterranean Sea. *Quat. Sci. Rev.* 73, 115–131.
- Grauel, A.L., Goudeau, M.-L.S., de Lange, G.J., Bernasconi, S.M., 2013b. Climate of the past 2500 years in the Central Mediterranean: a high-resolution climate reconstruction based on $\delta^{18}\text{O}$ and $\delta^{13}\text{C}$ of *G. ruber* (white). *The Holocene* 23 (10), 1440–1446.
- Grove, A.T., 2001. The “Little ice age” and its geomorphological consequences in Mediterranean Europe. *The Iceberg in the Mist: Northern Research in Pursuit of a “Little Ice Age”*, pp. 121–136.
- Hammer, Harper, D.A.T., Ryan, P.D., 2001. PAST-Palaeontological Statistics. www.uv.es/~pardomv/pe/2001_1/past/pastprog/past.pdf (Accessed Em 25 (07)).
- Haug, G.H., Günther, D., Peterson, L.C., Sigman, D.M., Hughen, K.A., Aeschlimann, P., 2003. Climate and the collapse of Maya civilization. *Science* 299 (5613), 1731–1735.
- Holzhauser, H., Magny, M., Zumbühl, H.J., 2005. Glacier and lake-level variations in west-central Europe over the last 3500 years. *The Holocene* 15 (6), 789–801.
- Hönsich, B., Allen, K.A., Lea, D.W., Spero, H.J., Eggins, S.M., deMenocal, P., Rosenthal, Y., Russell, A.D., Elderfield, H., 2013. The influence of salinity on Mg/Ca in planktic foraminifera-evidence from cultures, core-top sediments and complementary $\delta^{18}\text{O}$. *Geochim. Cosmochim. Acta* 121, 196–213.
- Hughen, K.A., Baillie, M.G.L., Bard, E., Beck, J.W., Bertrand, C.J.H., Blackwell, P.G., Buck, C.E., Burr, G.S., Cutler, K.B., Damon, P.E., Edwards, R.L., Fairbanks, R.G., Friedrich, M., Guilderson, T.P., Kromer, B., McCormac, G., Manning, S., Ramsey, C.B., Reimer, P.J., Reimer, R.W., Remmele, S., Southon, J.R., Stuiver, M., Talamo, S., Taylor, F.W., van der Plicht, J., Weyhenmeyer, C.E., 2004. Marine04 marine radiocarbon age calibration, 0–26 cal kyr BP. *Radiocarbon* 46 (3), 1059–1086.
- Hurrell, J.W., 1995. Decadal trends in the north Atlantic oscillation: regional temperatures and precipitation. *Science* 269 (5224), 676–679.
- Hut, G., 1987. Consultants’ Group Meeting on Stable Isotope Reference Samples for Geochemical and Hydrological Investigations: IAEA, Vienna 16–18 September 1985: Report to the Director General. International Atomic Energy Agency.
- Joannin, S., Brugiapaglia, E., de Beaulieu, J., Bernardo, L., Magny, M., Peyron, O., Goring, S., Vannière, B., 2012. Pollen-based reconstruction of Holocene vegetation and climate in southern Italy: the case of Lago Trifoglietti. *Clim. Past* 8, 1973–1996.
- Jochum, K.P., Weis, U., Stol, B., Kuzmin, D., Yang, Q., Raczek, I., Stracke, A., Birbaum, K.D.A., Frick, D., Günther, Enzweiler, J., 2011. Determination of reference values for NIST SRM 610–617 glasses following ISO guidelines. *Geostand. Geoanal. Res.* 35 (4), 397–429.
- Kaniewski, D., Paulissen, E., Van Campo, E., Weiss, H., Otto, T., Bretschneider, J., Van Lerberghe, K., 2010. Late second-early first millennium BC abrupt climate changes in coastal Syria and their possible significance for the history of the Eastern Mediterranean. *Quat. Res.* 74 (2), 207–215.

- Leider, A., Hinrichs, K.-U., Mollenhauer, G., Versteegh, G.J.M., 2010. Core-top calibration of the lipid-based and TEX⁸⁶ temperature proxies on the southern Italian shelf (SW Adriatic Sea, Gulf of Aranto). *Earth Planet. Sci. Lett.* 300 (1–2), 112–124 (11/15).
- Locarnini, R.A., Mishonov, A.V., Antonov, J.I., Boyer, T.P., Garcia, H.E., Baranova, O.K., Zweng, M.M., Johnson, D.R., Locarnini, R.A., Mishonov, A.V., Antonov, J.I., Boyer, T.P., Garcia, H.E., Baranova, O.K., Zweng, M.M., Johnson, D.R., 2010. *World Ocean Atlas 2009*. In: Levitus, S. (Ed.), NOAA Atlas NESDIS 68 Temperature vol. 1. U.S. Government Printing Office, Washington, D.C.
- Longinelli, A., Selmo, E., 2003. Isotopic composition of precipitation in Italy: a first overall map. *J. Hydrol.* 270 (1–2), 75–88.
- Magny, M., Bégeot, C., Guiot, J., Peyron, O., 2003. Contrasting patterns of hydrological changes in Europe in response to Holocene climate cooling phases. *Quat. Sci. Rev.* 22 (15), 1589–1596.
- Magny, M., Combouret-Nebout, N., de Beaulieu, J.L., Bout-Roumazielles, V., Colombaroli, D., Desprat, S., Francke, A., Joannin, S., Ortu, E., Peyron, O., Revel, M., Sadori, L., Siani, G., Sicre, M.A., Sammartin, S., Simonneau, A., Tinner, W., Vannière, B., Wagner, B., Zanchetta, G., Anselmetti, F., Brugiapaglia, E., Chapron, E., Debret, M., Desmet, M., Didier, J., Essallami, L., Galop, D., Gilli, A., Haas, J.N., Kallel, N., Millet, L., Stock, A., Turon, J.L., Wirth, S., 2013. North-south palaeohydrological contrasts in the Central Mediterranean during the Holocene: tentative synthesis and working hypotheses. *Clim. Past* 9, 2043–2071.
- Mann, M.E., Zhang, Z., Rutherford, S., Bradley, R.S., Hughes, M.K., Shindell, D., Ammann, C., Faluvegi, G., Ni, F., 2009. Global signatures and dynamical origins of the Little Ice Age and Medieval Climate Anomaly. *Science* 326 (5957), 1256–1260.
- Martín-Chivelet, J., Muñoz-García, M.B., Edwards, R.L., Turrero, M.J., Ortega, A.I., 2011. Land surface temperature changes in Northern Iberia since 4000 yr BP, based on $\delta^{13}\text{C}$ of speleothems. *Glob. Planet. Chang.* 77 (1), 1–12.
- Mayewski, P.A., Meeker, L.D., Twickler, M.S., Whitlow, S., Yang, Q., Lyons, W.B., Prentice, M., 1997. Major features and forcing of high-latitude northern hemisphere atmospheric circulation using a 110,000-year-long glaciochemical series. *J. Geophys. Res.* 102 (C12), 26345–26366.
- Mayewski, P.A., Rohling, E.E., Curt Stager, J., Karlén, W., Maasch, K.A., David Meeker, L., Meyerson, E.A., Gasse, F., van Kreveland, S., Holmgren, K., Lee-Thorp, J., Rosqvist, G., Rack, F., Staubwasser, M., Schneider, R.R., Steig, E.J., 2004. Holocene climate variability. *Quat. Res.* 62, 243–255.
- Morovic, M., Mati, F., Grbec, B., Dadi, V., Ivankovi, D., 2006. South Adriatic phenomena observable through VOS XBT and other ADRICOSM data. *Acta Adriat.* 47, 33–49.
- Nicault, A., Alleaume, S., Brewer, S., Carrer, M., P. N., Guiot, J., 2008. Mediterranean drought fluctuation during the last 500 years based on tree-ring data. *Clim. Dyn.* 31 (2–3), 227–245.
- Nieto-Moreno, V., Martínez-Ruiz, F., Giral, S., Jiménez-Espejo, F., Gallego-Torres, D., Rodrigo-Gámiz, M., García-Orellana, J., Ortega-Huertas, M., De Lange, G.J., 2011. Tracking climate variability in the Western Mediterranean during the Late Holocene: a multiproxy approach. *Clim. Past* 7 (4).
- Nieto-Moreno, V., Martínez-Ruiz, F., Giral, S., Gallego-Torres, D., García-Orellana, J., Masqué, P., Ortega-Huertas, M., 2013a. Climate imprints during the 'Medieval Climate Anomaly' and the 'Little Ice Age' in marine records from the Alboran Sea basin. *The Holocene* 23 (9), 1227–1237.
- Nieto-Moreno, V., Martínez-Ruiz, F., Willmott, V., García-Orellana, J., Masqué, P., Sinninghe Damsté, J.S., 2013b. Climate conditions in the westernmost Mediterranean over the last two millennia: An integrated biomarker approach. *Organic Geochemistry* 55, 1–10.
- Numberger, L., Hemleben, C., Hoffmann, R., Mackensen, A., Schulz, H., Wunderlich, J.M., Kucera, M., 2009. Habitats, abundance patterns and isotopic signals of morphotypes of the planktonic foraminifer *Globigerinoides ruber* (d'Orbigny) in the Eastern Mediterranean Sea since the marine isotopic stage 12. *Mar. Micropaleontol.* 73 (1), 90–104.
- Olsen, J., Anderson, N.J., Knudsen, M.F., 2012. Variability of the North Atlantic oscillation over the past 5,200 years. *Nat. Geosci.* 5 (11), 808–812.
- O'Neil, J.R., Clayton, R.N., Mayeda, T.K., 1969. Oxygen isotope fractionation in divalent metal carbonates. *J. Chem. Phys.* 51, 5547.
- Peyron, O., Goring, S., Dormoy, I., Kotthoff, U., Pross, J., de Beaulieu, J.-L., Drescher-Schneider, R., Vannière, B., Magny, M., 2011. Holocene seasonality changes in the Central Mediterranean region reconstructed from the pollen sequences of Lake Accesa (Italy) and Tenaghi Philippon (Greece). *The Holocene* 21 (1), 131–146.
- Peyron, O., Magny, M., Goring, S., Joannin, S., de Beaulieu, J.-L., Brugiapaglia, E., Sadori, L., Garfi, G., Kouli, K., Ioakim, C., Combouret-Nebout, N., 2013. Contrasting patterns of climatic changes during the Holocene across the Italian Peninsula reconstructed from pollen data. *Clim. Past* 9, 1233–1252.
- Pierre, C., 1999. The oxygen and carbon isotope distribution in the Mediterranean water masses. *Mar. Geol.* 153 (1), 41–55.
- Piervitali, E., Colacino, M., Conte, M., 1997. Signals of climatic change in the Central-Western Mediterranean basin. *Theor. Appl. Climatol.* 58 (3–4), 211–219.
- Piva, A., Asiola, A., Trincardi, F., Schneider, R.R., Vigliotti, L., 2008. Late-Holocene climate variability in the Adriatic Sea (Central Mediterranean). *The Holocene* 18 (1), 153–167.
- Pla, S., Catalan, J., 2005. Chrysophyte cysts from lake sediments reveal the submillennial, winter/spring climate variability in the northwestern Mediterranean region throughout the Holocene. *Clim. Dyn.* 24 (2–3), 263–278.
- Poulain, P.-M., 2001. Adriatic Sea surface circulation as derived from drifter data between 1990 and 1999. *J. Mar. Syst.* 29 (1–4), 3–32 (5).
- Pujol, C., Vergnaud Grazzini, C., 1995. Distribution patterns of live planktic foraminifers as related to regional hydrography and productive systems of the Mediterranean Sea. *Mar. Micropaleontol.* 25 (2), 187–217.
- Raich, F., 1996. On the fresh balance of the Adriatic Sea. *J. Mar. Syst.* 9 (3–4), 305–319 (12).
- Reichart, G.-J., Jorissen, F., Anschutz, P., Mason, P.R.D., 2003. Single foraminiferal test chemistry records the marine environment. *Geology* 31 (4), 355–358.
- Rohling, E.J., 2000. Paleosalinity: confidence limits and future applications. *Mar. Geol.* 163 (1), 1–11.
- Rohling, E.J., Pälike, H., 2005. Centennial-scale climate cooling with a sudden cold event around 8,200 years ago. *Nature* 434 (7036), 975–979.
- Rohling, E.J., Mayewski, P.A., Abu-Zied, R.H., Casford, J.S.L., Hayes, A., 2002. Holocene atmosphere-ocean interactions: records from Greenland and the Aegean Sea. *Clim. Dyn.* 18 (7), 587–593.
- Rohling, E.J., Sprovieri, M., Cane, T., Casford, J.S.L., Cooke, S., Bouloubassi, I., Emeis, K.C., Schiebel, R., Rogerson, M., Hayes, A., Jorissen, F.J., Kroon, D., 2004. Reconstructing past planktic foraminiferal habitats using stable isotope data: a case history for Mediterranean sapropel S5. *Mar. Micropaleontol.* 50 (1), 89–123.
- Rohling, E.J., Hayes, A., Mayewski, P.A., Kucera, M., 2009. Holocene climate variability in the Eastern Mediterranean, and the end of the Bronze Age. In: Bachhuber, C., Roberts, R.G. (Eds.), *Forces of Transformation: The End of the Bronze Age in the Mediterranean*. BANE Publication Series 1. Oxbow Books, Oxford, pp. 2–5 (ISBN-13: 978-1-84217-332-9).
- Rosenthal, Y., Boyle, E.A., Labeyrie, L., 1997. Last glacial maximum paleochemistry and deepwater circulation in the southern ocean: evidence from foraminiferal cadmium. *Paleoceanography* 12 (6), 787–796.
- Rosenthal, Y., Field, M.P., Sherrell, R.M., 1999. Precise determination of element/calcium ratios in calcareous samples using sector field inductively coupled plasma mass spectrometry. *Anal. Chem.* 71 (15), 3248–3253.
- Rosenthal, Y., Morley, A., Barras, C., Katz, M.E., Jorissen, F., Reichart, G.J., Oppo, D.W., Linsley, B.K., 2011. Temperature calibration of Mg/Ca ratios in the intermediate water benthic foraminifer *Hyalina balthica*. *Geochim. Geophys. Geosyst.* 12 (4) (Q04003).
- Ruff, M., Wacker, L., Gäggeler, H.W., Suter, M., Synal, H.A., Szidat, S., 2007. A gas ion source for radiocarbon measurements at 200 kV. *Radiocarbon* 49 (2), 7–307.
- Sangiorgi, F., Capotondi, L., Combouret Nebout, N., Vigliotti, L., Brinkhuis, H., Giunta, S., Lotter, A.F., Morigi, C., Negri, A., Reichart, G.-J., 2003. Holocene seasonal sea-surface temperature variations in the southern Adriatic Sea inferred from a multiproxy approach. *J. Quat. Sci.* 18 (8), 723–732.
- Schmidt, G.A., 1999. Error analysis of paleosalinity calculations. *Paleoceanography* 14 (3), 422–429.
- Schmidt, G.A., Biggs, G.A., Rohling, E.J., 1999. Global Seawater Oxygen-18 Database. <http://data.giss.nasa.gov/o18data/>.
- Schroeter, J.S., 1783. *Einleitung in die conchylienkenntniss*. Nach Linne 1, 860.
- Sellschopp, J., Álvarez, A., 2003. Dense low-salinity outflow from the Adriatic Sea under mild (2001) and strong (1999) winter conditions. *J. Geophys. Res.* 108 (C9), 8104.
- Shackleton, N.J., 1974. Attainment of isotopic equilibrium between ocean water and the benthonic foraminifera genus *Uvigerina*: isotopic changes in the ocean during the last glacial. *Colloques Internationaux du C.N.R.S.* 219, 203–213.
- Shanahan, T.M., Overpeck, J.T., Anchukaitis, K.J., Beck, J.W., Cole, J.E., Dettman, D.L., Peck, J.A., Scholz, C.A., King, J.W., 2009. Atlantic forcing of persistent drought in west Africa. *Science* 324 (5925), 377–380.
- Shapiro, S.S., Wilk, M.B., 1965. An analysis of variance test for normality (complete samples). *Biometrika* 52 (3/4), 591–611.
- Siani, G., Magny, M., Paterne, M., Debret, M., Fontugne, M., 2013. Paleohydrology reconstruction and Holocene climate variability in the South Adriatic Sea. *Clim. Past* 9 (1), 499–515.
- Snedecor, G.W., Cochran, W.G., 1989. *Statistical Methods*. eighth edition. Iowa State University Press, Ames, Iowa.
- Spero, H.J., 1992. Do planktic foraminifera accurately record shifts in the carbon isotopic composition of seawater ΣCO_2 ? *Mar. Micropaleontol.* 19 (4), 275–285.
- Spero, H.J., Williams, D.F., 1989. Opening the carbon isotope "vital effect" black box 1. seasonal temperatures in the euphotic zone. *Paleoceanography* 4 (6), 593–601.
- Synal, H.-A., Stocker, M., Suter, M., 2007. MICADAS: a new compact radiocarbon AMS system. *Nucl. Inst. Methods Phys. Res. B* 259 (1), 7–13 (6).
- Stine, S., 2000. On the Medieval climatic anomaly. *Current Anthropology* 41, 627–628.
- Trigo, R., Xoplaki, E., Zorita, E., Luterbacher, J., Krichak, S.O., Alpert, P., Jacobeit, J., Sáenz, J., Fernández, J., González-Rouco, F., García-Herrera, R., Rodo, X., Brunetti, M., Nanni, T., Maugeri, M., Türke, M., Gimeno, L., Ribera, P., Brunet, M., Trigo, I.F., Crepon, M., Mariotti, A., 2006. Chapter 3. Relations between variability in the Mediterranean region and mid-latitude variability. In: Lionello, P., Boscolo, P.M.R., R. (Eds.), *Developments in Earth and Environmental Sciences*. Elsevier, pp. 179–226.
- Trouet, V., Esper, J., Graham, N.E., Baker, A., Scourse, J.D., Frank, D.C., 2009. Persistent positive North Atlantic oscillation mode dominated the Medieval Climate Anomaly. *Science* 324 (5923), 78–80.
- Turchetto, M., Boldrin, A., Langone, L., Misserocchi, S., Tesi, T., Foglini, F., 2007. Particle transport in the Bari canyon (southern Adriatic Sea). *Mar. Geol.* 246 (2–4), 231–247 (12/7).
- Versteegh, G.J.M., de Leeuw, J.W., Taricco, C., Romero, A., 2007. Temperature and productivity influences on U^{37}K and their possible relation to solar forcing of the Mediterranean winter. *Geochim. Geophys. Geosyst.* 8 (9).
- Waelbroeck, C., Mulitza, S., Spero, H., Dokken, T., Kiefer, T., Cortijo, E., 2005. A global compilation of late Holocene planktonic foraminiferal $\delta^{18}\text{O}$: relationship between surface water temperature and $\delta^{18}\text{O}$. *Quat. Sci. Rev.* 24 (7), 853–868.
- Wang, Y., Cheng, H., Edwards, R.L., He, Y., Kong, X., An, Z., Wu, J., Kelly, M.J., Dykoski, C.A., Li, X., 2005. The Holocene Asian monsoon: links to solar changes and North Atlantic climate. *Science* 308 (5723), 854–857.

- Wanner, H., Beer, J., Bütikofer, J., Crowley, T.J., Cubasch, U., Flückiger, J., Goosse, H., Grosjean, M., Joos, J.O., Kaplan, M., Küttel, S.A., Müller, I.C., Prentice, O., Solomina, T.F., Stocker, P., Tarasov, M., Wagner, F., Widmann, M., 2008. Mid- to Late Holocene climate change: an overview. *Quat. Sci. Rev.* 27 (19–20), 1791–1828.
- Wanner, H., Solomina, O., Grosjean, M., Ritz, S.P., Jetel, M., 2011. Structure and origin of Holocene cold events. *Quat. Sci. Rev.* 30 (21), 3109–3123.
- Weiss, B., 1982. The decline of late Bronze Age civilization as a possible response to climatic change. *Clim. Chang.* 4 (2), 173–198.
- Weldeab, S., Lea, D.W., Schneider, R.R., Andersen, N., 2007. 155,000 years of west African monsoon and ocean thermal evolution. *Science* 316 (5829), 1303–1307.
- Wit, J.C., Reichert, G.-J., Jung, S.J.A., Kroon, D., 2010. Approaches to unravel seasonality in sea surface temperatures using paired single-specimen foraminiferal $\delta^{18}\text{O}$ and Mg/Ca analyses. *Paleoceanography* 25 (PA4220).
- Wit, J.C., de Nooijer, L.J., Barras, C., Jorissen, F.J., Reichert, G.J., 2012. A reappraisal of the vital effect in cultured benthic foraminifer *Bulimina marginata* on Mg/Ca values: assessing temperature uncertainty relationships. *Biogeosciences* 9, 3693–3704.
- Wit, J.C., de Nooijer, L.J., Wolthers, M., Reichert, G.J., 2013. A novel salinity proxy based on Na incorporation into foraminiferal calcite. *Biogeosciences* 10, 6375–6387.
- Zonneveld, K.A.F., et al., 2008. Report and preliminary results of R/V POSEIDON cruise P339, Piräus – Messina, 16 June–2 July 2006. CAPPUCINO – Calabrian and Adriatic Palaeoproductivity and Climatic Variability in the Last Two Millennia. *Berichte, Fachbereich Geowissenschaften* 268.
- Zonneveld, K.A.F., Chen, L., Möbius, J., Mahmoud, M.S., 2009. Environmental significance of dinoflagellate cysts from the proximal part of the Po-river discharge plume (off southern Italy, Eastern Mediterranean). *J. Sea Res.* 62 (4), 189–213.